Molecular Communication Model for Targeted Drug Delivery in Multiple Disease Sites with Diversely Expressed Enzymes

Uche A.K. Chude-Okonkwo*, Reza Malekian, and B.T. Maharaj

***Abstract*— Targeted drug delivery (TDD) for disease therapy using liposomes as nanocarriers has received extensive attention in the literature. The liposome's ability to incorporate capabilities such as long circulation, stimuli responsiveness and targeting characteristics, makes it a versatile nanocarrier. Timely drug release at the targeted site requires that trigger stimuli such as pH, light and enzymes be uniquely overexpressed at the targeted site. However, in some cases, the targeted sites may not express trigger stimuli significantly, hence, achieving effective TDD at those sites is challenging. In this paper, we present a molecular communication-based TDD model for the delivery of therapeutic drugs to multiple sites that may or may not express trigger stimuli. The nanotransmitter and nanoreceiver models for the molecular communication system are presented. Here, the nanotransmitter and nanoreceiver are injected into the targeted body system's blood network. The compartmental pharmacokinetics model is employed to model the transportation of these therapeutic nanocarriers to the targeted sites where they are meant to anchor before the delivery process commences. We also provide analytical expressions for the delivered drug concentration. The effectiveness of the proposed model is investigated for drug delivery on tissue surfaces. Results show that the effectiveness of the proposed molecular communication-based TDD depends on parameters such as the total transmitter volume capacity, the receiver radius, the diffusion characteristic of the microenvironment of the targeted sites, and the concentration of the enzymes associated with the nanotransmitter and the nanoreceiver designs.**

***Index Terms*—Molecular communication, Targeted drug delivery, liposomes, enzymes, nanomedicine.**

I. Introduction

In recent times, there has been increasing interest in the application of nanotechnology concepts, tools and devices to improve existing technologies as well as introduce entirely new technological innovations. Nanotechnology dwells on the concept of manipulating materials at the particulate and molecular levels of systems, and has found potential applications in many areas. A nanotechnology application of concern in this work is nanomedicine [1], which gears towards improving medical and healthcare systems using nano-scale concepts, devices, tools and techniques. Nanomedicine exploits the unique properties of nanomaterials for applications as diverse as targeted drug delivery (TDD), magnetic resonance imaging (MRI) contrast enhancement, gene therapy, biomarkers and many others [2].

In recent times a branch of nanotechnology that has been attracting lots of attention is the molecular communication (MC) [3]. MC is a new communication paradigm that uses biochemical signals to achieve information exchange among naturally and artificially created bio-nano scale devices over short distances. MC promotes the idea of systemized cooperation among nanodevices for efficient task handling. The emergence of MC has found potential applications in fields that include bioengineering [4-7], nanomedicine [7-12], and environmental safety [13]. This paper focuses on the application of MC to the field of nanomedicine, and specifically TDD.

TDD is an engineered approach for targeting and delivering drugs to specific areas of the body in a controlled manner using nanocarriers. The approach is geared towards ensuring that therapeutic drugs are localized to a specific part of the body without affecting other healthy parts of the body where they will otherwise produce adverse effects. It is also aimed at minimizing drug degradation and loss. The idea of TDD is nowadays under intensive study as it is at the cutting edge of modern medical therapeutics [14, 15] and has found applications in areas such cancer therapy [16] and thrombosis therapy [17]. The transport of drug particles in the human body and delivery to a specific tissue or organ can be viewed in the context of MC. In this sense, the drug particle injection device is the transmitter, the drug particles are information carriers, the blood vessel network is the communication channel, and the targeted tissue, the receiver [10].

In most TDD scenarios, for specificity in targeting, the transported drug particles or other therapeutic molecules are encapsulated in what is termed *nanocarrier*. The commonly used nanocarriers for TDD include liposome, micelle and dendrimer [18]. These nanocarriers are engineered in such a way that they encapsulate drug particles, which they deliver to a specific location in the body after being injected into the body. The TDD nanocarrier of concern in this work is the liposome. The liposome is a biocompatible, biodegradable nanocarrier that has extensively been studied as a promising

drug delivery model for bioactive compounds in cancer therapy [19-21]. The ability of liposome to incorporate capabilities such as long circulation, internal/external stimuli responsiveness and targeting characteristics, makes it a versatile nanocarrier. The long circulation property is due to the possibility of incorporating hydrophilic polymers such as poly-(ethylene glycol) (PEG) into its membrane, which gives it a stealthy characteristic. However, to be able to release encapsulated drug at the targeted site and given time instant, the liposome will also incorporate degradable polymers, which on the action of certain stimuli, degrade and cause the release of the encapsulated drug. Such stimuli include pH, temperature, light, ultrasound, magnetic fields and enzymes [22]. With the stimuli-responsive capability, it is possible to design liposomes that deliver drugs to specific sites where the trigger stimulus is present or overexpressed. Such approach has been a subject of intensive research in cancer therapy where liposomal content release is triggered by a conducive pH at the tumor site [23], and enzymes such as matrix metalloproteinases (MMP) that are overexpressed at tumor sites [24]. In an effort to further improve drug release performances, novel multi-stimuli responsive polymeric nanoparticles that respond to a combination of two or more signals have been proposed in [25].

Ideally, before the liposome can release its content, it needs to specifically target and position itself on the target site. This task is achieved by incorporating target ligands that can bind to specific receptor located at the targeted site, with high affinity [26].

A. Problem Definition

To provide a clear statement as to the issues this paper addresses, we shall discuss an illustrative application scenario. Let Fig. 1 depict a scenario where more than one tissue is to be administered with drugs using targeted delivery approach. In this illustration, we arbitrarily consider three different tissue sites *A*, *B*, and *C* for targeting. To use conventional triggered liposome-based targeted drug delivery approach [27, 28] will require that the drug-carrying liposome anchors and releases the drugs at each of the sites. This is an effective approach if all the sites overexpress enzymes that can act as stimuli for the release of the drugs encapsulated by the liposome. However, this is not often the case as some stimuli enzymes may be overexpressed at both the targeted and non-targeted sites in the body. In fact, the main disadvantage of enzyme-triggered release is that no enzyme is solely expressed in the targeted region; as such non-specific release occurs throughout the body [29]. More also, in some cases, the trigger stimuli may not be significantly expressed at the targeted site. This is often the case when a disease is at its early stage or with improved survival. For instance, such situation arise in the use of MMP as a responsive release stimuli in tumor therapy, where the level of MMP expression depends on the state or survival level of the tumor [30]. In these circumstances, the conventional triggered liposome-based targeted drug delivery approach fails. This work addresses this challenge.

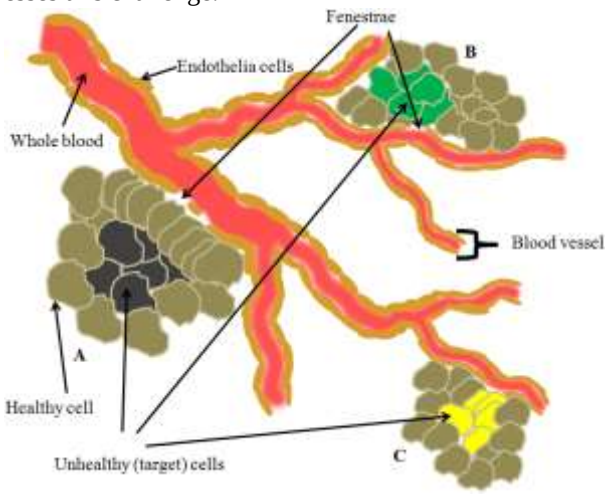

Fig. 1. Illustration of multiple sites targeted for drug delivery scenario.

Let us reasonably assume that all three sites express surface receptors for targeting. Such is the scenario in cancer cells where folate receptors are commonly overexpressed in many human cancers [31]. We also assume that the targeted sites express different or no stimuli for triggered content release. The membrane of the drug-carrying vessel must be coated with target ligands for binding to the surface receptors. Hence, the liposomes can anchor at the different target sites, but content-release cannot be achieved at sites where stimuli enzymes are not significantly expressed. The issue now is how to ensure that nanocarriers that anchor at the sites release drugs even if the sites express no release stimuli. This is the circumstance and challenge that this paper focuses on.

In this paper, we specifically address the following challenge. *How do we model a liposome-based drug delivery system that can simultaneously deliver therapeutic drugs to different targeted sites where some or all the sites do not significantly express stimuli-enzymes for triggered drug release*? We address this challenge by looking to MC for inspiration. We present MC-based system model for achieving TDD at multiple target sites in which stimuli for triggered-release are not significantly expressed. We model a molecular transmitter that emits drug molecules in response to the presence of a specific trigger molecule that is uniformly introduced at all targeted sites. This transmitter consists of drug carrying enzyme-triggered liposomes encased in a lipid membrane structure. Ordinarily, the transmitter can encapsulate active drugs that will be directly released at the targeted sites upon being externally triggered. However, there is the possibility that the transmitter may encounter catastrophic failure in the blood network before getting to the targeted site, thereby releasing active drugs that undesirably intoxicate the system. Hence, to ensure that only potent drugs are delivered to the targeted sites, the transmitter model is such that the liposome-encapsulated drugs are inactive in the form of prodrugs. In this case, even if the transmitter

encounters catastrophic failure *en route* to the targeted sites, only inactive drugs will be deposited at non-targeted sites. The inactive drug molecules released by the nanotransmitter are then activated by a complementary nanoreceiver. Such approach is presented in [11] within the context of MC. In this paper, following [11] we model the receiver as consisting of enzymes that activate the released prodrugs (inactive drugs). But in contrast to the model in [11], the receiver is also fettered with specific ligands for high affinity binding to receptors at the targeted sites. The transport of the transmitters and receivers to the targeted site is modeled as a pharmacokinetic process that is based on the multi-compartment model [32]. The performance evaluation of the proposed MC-based TDD system for multiple site application is analysed in terms of the nanotransmitter and nanoreceiver parameters. For the rest of this work except otherwise stated, the term nanocarrier is used to imply either the nanotransmitter or the nanoreceiver. The term nanoparticle is used henceforth to imply all molecules/ particles of nano scale size, which includes the nanocarriers. The terms prodrug is used interchangeably with inactive drug.

The rest of this paper is organized as follows. The review of related works in MC and liposome-based TDD is presented in Section II. The proposed system model is presented in Section III. In Section IV, the pharmacokinetics and targeting models for the transportation of the nanoparticles to the targeted sites are presented. The drug release and emission characteristics at the targeted sites are modeled in Section V. In Section VI, the drug reception model is presented. The sequence and timing optimization of the nanoparticles' injection into the body system is discussed VII. Finally, simulation results and discussion are presented in Section VIII.

II. Review of Related Works in MC and Liposome-based TDD

In [33], a review of the state of the art in MC is presented with emphasis on the opportunities and challenges in MC research. In [34], some first insights about security and privacy aspects of MC systems is presented by highlighting the open issues, challenges and some specific directions of potential solutions. A bio-inspired layered architecture of MC system that follows the traditional layered architecture of contemporary electronic communication, and a discussion on research issues in MC are presented in [35]. In [36], a review of the application of MC to healthcare delivery can be found. By using system-theoretic representation, MC propagation models that include the influence of surface receptors and enzymes are presented in [37].

Contemporary works that present the concept of drug delivery in the context of MC can be found in [10, 11, 38-40]. In [10], an MC-based drug propagation network model that is built upon the solution to Navier-Stokes equation is presented. This model uses transmission line theory and the concept of harmonic transfer matrix developed in [41] to model the branches of a typical blood vessel network. The analysis of the noise and capacity of the model in [10] is presented in [42]. A model for diffusion-controlled MC that is applied to targeted drug delivery where inactive drug particles are transmitted and received/processed by mean of enzyme-catalyzed is presented. An enzyme-catalysis model for the MC-based TDD architecture is presented in [11]. This model also derived analytical expressions for information transfer for accessing the influence of some basic nanocarrier design parameters on the TDD system performance. In [39], within the context of MC, a bottom-up approach of modelling the propagation of antibodies for the purpose of antibody-mediated drug delivery (ADD) is presented. The essence of the ADD system is to use artificial molecules that are constructed from biological materials to build and engineer drug delivery systems [43]. In [40], through MC paradigm a pharmacokinetic model for modelling and estimating the biodistribution of drug-loaded particles in presented. This model also employed the harmonic transfer matrix to propose the application of the MC abstraction to model drug pharmacokinetics, biodistribution estimation and optimization of the drug injection rate in TDD. Based on MC paradigm, a transmission rate control problem is formulated in [44], which finds application in reducing rate loss in drug delivery application. In [45], a TCP-like communication protocol for MC is presented, which finds application in drug delivery. In [46], the concept of congestion in diffusion-based MC for drug delivery application is introduced. And a model for illustrating and analysing the dynamical behaviour of the congestion phenomenon is also proposed in [46].

In the context of liposome-based TDD, most contemporary works present and discuss the idea outside the perspective of MC. Nevertheless, we review some existing literatures in the open domain that is closely related and support the ideas in this present work with respect to liposome-based TDD. In [47], different types of liposome-based nanocapsules are developed for addressing the stability concern of nanocarriers. Typically, for a liposome to actively release its content, it must be triggered by stimuli that degrade its membrane. Commonly explored stimuli include pH, temperature, magnetic, light, acoustic, and enzymes [27, 48]. This present work focuses on the use of enzymes to trigger release of liposome content. This mode of release basically takes advantage of the altered expression profile of specific enzymes observed in pathological conditions, such as cancer or inflammation [48]. A review of recent works in enzyme-triggered liposome for TDD can be found in [49, 50]. Popular enzymes for triggered release include MMPs, which are significantly expressed in tumors [51, 52], and have found application in cancer therapy [24, 53]. The general literature on liposome-based TDD assumes the overexpression of enzymes such as MMPs for triggered release. However, it has been shown in [54] that the expression level of MMP-9 depends on the stage of the cancer, which positively correlates

with tumor metastasis and depth of tumor invasion; and the aggressive behavior and progression of cancer. MMP expression has been reported to be low or undetectable in most benign elements but is substantially increased in a majority of human malignancies [55-57]. And in [53] it was demonstrated that cancer cells, which secrete low levels of MMP-9 failed to release significant amount of the liposomal contents.

III. Proposed TDD System Model for Multisite Delivery

A. Proposed System Model

The block diagram of the proposed TDD model for multiple site targeting is shown in Fig. 2. Here, specific nanoparticles are injected into the cardiovascular system represented by the *body or blood channel* block. These nanoparticles include liposome-based nanocarriers acting as the nanotransmitter (Nano-T), the nanoreceiver (Nano-R) for activating the released liposome drug content, and trigger molecules for activating the drug delivery system. The architecture and release mechanism of the proposed Nano-T and the model of the Nano-R will be presented shortly. On injection, these nanoparticles whose concentration is represented by $I(t)$ propagate through the blood vessel network in the presence of noise, and enter the targeted region through the extracellular matrix (ECM). The particles exit the blood vessel through the endothelia gaps on the surface of the vessel called fenestrae. The level of permeability increases with the level of fenestrations. The fenestrae are typically modeled as narrow pores perpendicular to the vessel wall. Fenestration diameter of 60 nm is typical for normal vessels and 240 -400 nm for tumor vessels [58, 59].

In this model, for effectiveness, the Nano-T and Nano-R are first injected into the system for reasons that will be discussed in Section VII. On reaching any of the targeted sites, the Nano-T and Nano-R anchor at the sites by binding to the cells' receptors with the complementary ligands fettered to their surfaces. The total number of the nanocarriers that anchors at each of the sites is denoted by $a_n(t)$, n = 2, 3,.., N, where N is a real number and N-1 is the total number of the targeted sites. The pharmacokinetics model for determining $a_n(t)$ is presented in Section IV.

With the Nano-Ts and Nano-Rs at the target sites, a certain concentration of trigger molecule is injected into the system to prompt the start of the drug delivery process. The trigger molecules traverse through the blood vessel and into the targeted areas, where they bind to certain receptors on the surface of the Nano-T to activate the prodrug release process. The released prodrug concentration $g_n(t, r_0)$, n = 2, 3,.., N, which is the molecular flux out of the Nano-T surface in site n, is defined at a reference position r_0 and time t. The released prodrug molecules diffuse to the Nano-R space, where they are activated by the immobilized enzymes on the surface of the Nano-R. We designate the output of the tissue channel as $\psi_n(t)$, n = 2, 3,.., N, and the concentration of the drugs delivered to the sites as $y_{T,n}(t)$, n = 2, 3,..,N.

B. Proposed Nanotransmitter Model

The proposed MC transmitter architecture is shown in Fig. 3 and 4. It essentially composes of a lipid membrane. The membrane of this structure is equipped with synthetic nanopores [60-62] through which entrapped molecules can leave its interior, and receptor proteins for triggering the transmission mechanism. The receptors serve as the input molecular antenna, while the nanopores are the output molecular antenna through which prodrug molecules transude into the propagation microenvironment. To enable the capability of the transmitter to target and anchor at each of the tissue sites, the membrane is also grafted with specific ligands mounted on the tip of PEG linked to the membrane, which binds to complimentary receptors at each of the targeted tissues. These target ligands are assumed unique to receptors found at each tissue site. Examples of popular ligands for targeting include sugar, folic acid, peptide and antibody [63]. And some corresponding complementary receptors include folate, peptide and cell surface antigen. These receptors are

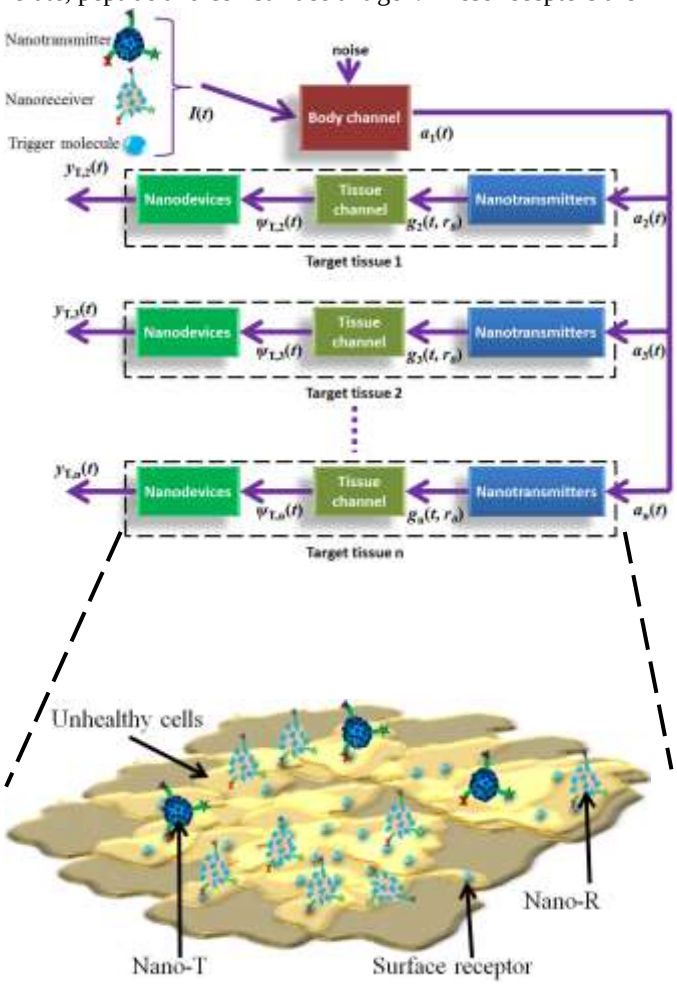

Fig. 2. Scheme of the bio-inspired MC system model for TDD.

intrinsically expressed profusely in different states of a

disease. For instance, the folate receptor is an attractive target for selective tumour delivery of liposomal doxorubicin because it is abundantly expressed in a large percentage of tumour cells.

Inside the transmitter are liposomes that encapsulate the prodrug molecules. The liposomes are coated with poly-amino acid (PAA) that can be degraded by the hydrolysis action of a liposomal protease (LP). When LP cleaves the PAA, the PAA coatings on the liposome are degraded thereby causing the release of the entrapped prodrug molecules, which subsequently diffuse into the micro-environment (tissue channel) through the nanopores. To ensure that the LP does not cleave the PAA coating before the start of transmission, they have to exist as zymogens right before they are activated. The LPs are typically activated by being cleaved by proteolytic enzymes *E*, which are associated with the intracellular (inside the transmitter) section of the transmitter surface receptors. Also, to avoid the escape of the LPs through the nanopores before activation, size-exclusion biomolecules separation concept is employed. This implies that the size of the protease should be larger than that of the pores'. The nanopores size-exclusion capability has been considered in [70] as a support for kidney cells, and as a blood filter that retains serum proteins while allowing smaller waste substances out.

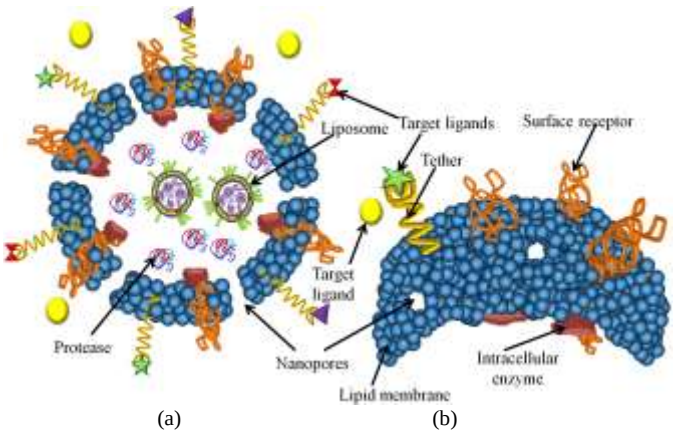

Fig. 3. Schematic representation of (a) the molecular transmitter (b) top view of the transmitter. *This diagram is best viewed in color*.

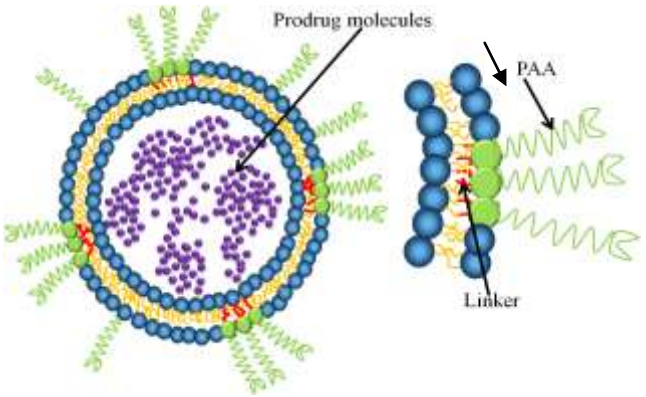

Fig. 4. Schematic representation of the PAA coated liposome encapsulating drug molecules. *This diagram is best viewed in color*.

The reaction kinetics of the transmission steps are summarized as follows. The ligand-receptor binding reaction kinetics that triggers the transmission operation can be modeled as

$$L + R \underset{kk_{-1}}{\overset{kk_1}{\leftrightarrow}} RL \tag{1}$$

where L is the trigger molecule, R is the surface receptor, RL is the receptor-trigger molecule complex and, kk_1 and kk_{-1} are positive rate constants. The ensuing receptor-ligand complex-initiated protease activation kinetics is given by

$$RL + E \overset{\alpha_1}{\rightarrow} RLE \overset{\alpha_2}{\rightarrow} RL + E^* \tag{2}$$

$$P_I + E^* \overset{\alpha\alpha_1}{\rightarrow} P_I E^* \overset{\alpha\alpha_2}{\rightarrow} P_A + E^* \tag{3}$$

where E is the inactive intracellular enzyme associated with the surface receptor R, E^* is the active version of E, P_I is the inactive liposomal protease, $P_I E^*$ is the enzyme-protease complex and P_A is the active protease. The terms α_1, $\alpha\alpha_1$, α_2 and $\alpha\alpha_2$ are positive rate constants.

In the presence of P_A, the cleaving of the r PAA coatings Z can be modeled as

$$P_A + Z \underset{\beta_{-1}}{\overset{\beta_1}{\leftrightarrow}} P_A Z \overset{\beta_2}{\rightarrow} P_A + I_M \tag{4}$$

where $P_A Z$ is the protease-PAA complex, I_M is the cleaved PAA molecules. The terms β_1, β_{-1} and β_2 are positive rate constants. When a certain concentration of the PAA is cleaved, the liposome stability is compromised, and the drug particles are released.

Let us denote the released drug particle as G. These particles diffuse into the tissue medium through the nanopores. Hence, the emission characteristics of the Nano-T can be expressed as a function of the transmitted molecule size r_M, the nanopores size r_N, the distribution f_N of the nanopores over transmitter surface ∂_Ω , and the ratio of the nanopores footprint to ∂_Ω. Technically, the parameters r_M , r_N, f_N and ∂_Ω define the possibility of a diffusing molecules at an arbitrary time t being reflected back at some boundary points at the transmitter surface. In reference to Fig. 2, following [Equation (1), 77], and for a specific trigger input signal $T(t)$, we can therefore express the emitted concentration of G, $g(t_0,r_0)$ as

$$T(t) \xrightarrow{\wp, r_M, r_N, f_N, \partial_\Omega} g_n(t, r_0) \tag{5}$$

where t_0 and r_0 are reference time and position, respectively. The term $\wp$ is defined by the activities in (1)-(4).

Implementation Issues: Some existing techniques that can be employed to synthesize this type of nanotransmitter are presented in [60, 62, 64-67]. Interestingly, nanoporous membranes with well-controlled pore size, porosity and membrane thickness offer an attractive route for making capsules that may be used to provide controlled release of pharmacologic agents [68]. Nanoporous inorganic membranes have been tested for sustained release of ophthalmic drugs to treat conditions related to the eye [69]. When coupled to bio-

sensors, smart drug delivery systems that respond to physiological conditions could be developed.

As was earlier mentioned, the liposomes of interest in this work are those whose release is triggered by the cleaving of their PEGylated coatings. It is required that just like the protease the sizes of these liposomes must be larger than the nanopores' to prevent them from escaping through the nanopores before transmission is initiated. For the preparation methods for such liposome, the reader shall refer to [71-76] and the references therein for detailed information. For the rest of this work, it is assumed that the molecules that diffuse across the Nano-T membrane have negligible effect on the processes that go on inside the transmitter.

C. Proposed Nanoreceiver Model

The architecture of the Nano-R is shown in Fig. 5(a). It primarily composes of lipopeptide membrane covered with enzymes and some target-ligands for targeting. Typically, the emitted prodrug particle G diffuses through the tissue channel to Nano-R and binds to enzymes resulting in their transformation to an active state as shown in Fig. 5(b). For a given concentration of the emitted inactive drug molecules $g(t,r_0)$, we can therefore express the concentration of the inactive drug molecules received within a conceptual reception space [78] around the Nano-R as

$$g_n(t,r_0) \xrightarrow{D,r,r_R} \psi_n(t) \tag{6}$$

where D is the diffusion coefficient of the diffusion channel, r is the transmit-receive distance, and r_R is the receiver radius.

As the active drug molecules are formed by the enzymatic reaction between the surface enzymes and the prodrug molecules, they diffuse across the targeted tissue(s). Hence, we can express the delivered concentration of the active drug molecules as

$$\psi_n(t) \xrightarrow{q_0,\aleph} y_{Tn}(t) \tag{7}$$

where q_0 is the concentration of the surface enzymes and $\aleph$ is the vector of the reaction constants involved in the enzymatic reaction. The drug activation kinetic can be expressed as

$$G + E_R \underset{\xi_{-1}}{\overset{\xi_1}{\leftrightarrow}} Y_I E_R \xrightarrow{\xi_2} E_R + Y_A \tag{8}$$

where E_R is the receiver surface enzyme, $Y_I E_R$ is the complex formed by G and E_R, and Y_A is the active drug. The terms ξ_1, $\xi_{-1}, \xi_2 \in \aleph$ are rate constants.

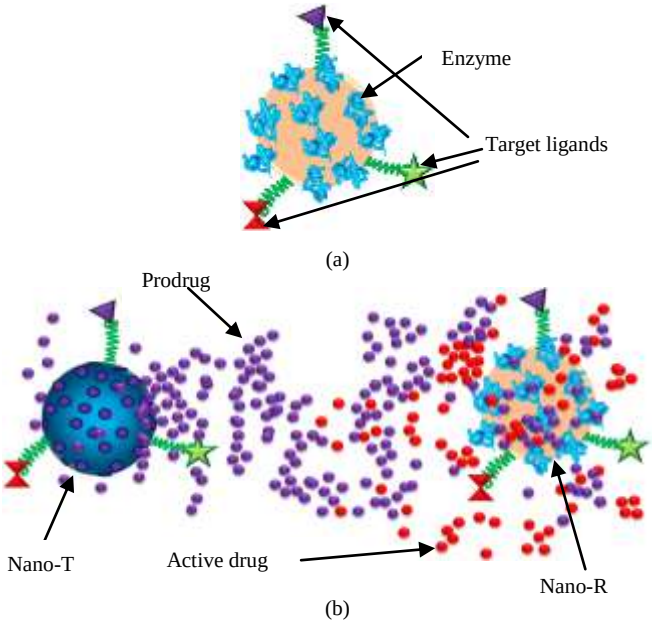

Fig. 5. (a) A schematic diagram of the Nano-R (b) An illustration of the proposed molecular communication system for TDD. *This diagram is best viewed in color*.

IV. Pharmacokinetic and Targeting Models

In this section, we present the pharmacokinetic model of the course of the nanoparticles from the point of injection to their location at the targeted sites. We also present the model for the anchoring of the nanocarriers on the tissue surface.

A. Pharmacokinetic Model

We employ the compartment model to delineate the number of the nanoparticles that are eventually resident at the targeted sites after being injected. A schematic overview of the compartment model is depicted in Fig. 6. In employing this model the following assumptions are made. 1) The rate of nanoparticles movement between compartments obeys a first-order reaction law, which is biophysically supported for a number of natural phenomena such as diffusion 2) The system is a well-mixed one. This entails the instant homogeneous distribution of nanoparticles within the compartments. 3) The nanocarriers do not undergo chemical reactions on their course to the targeted sites. 4) The volumes of the compartments do not vary with time. 5) The drug is completely eliminated from the body through the blood compartment.

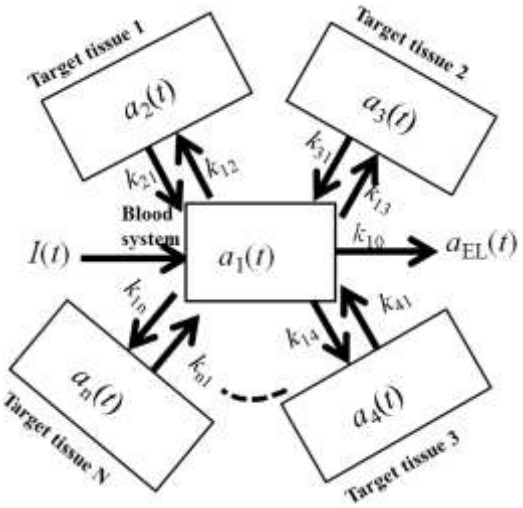

Fig. 6. Mammillary multi-compartment model architecture.

Let the volumes of the compartments be V_n, n = 1,2,…,N. The concentration of the nanoparticles in each compartment is given by the ratio of the number of nanoparticles a_n to V_n. The central compartment is the blood system with number of nanoparticles designated by $a_1(t)$. The function $a_{EL}(t)$ is the number of eliminated nanoparticles over time as a function of the elimination rate k_{10}. This number includes those that undergo phagocytosis. The parameters k_{1n} and k_{n1} are first-order rate constant in or out of the compartments, respectively. These rate constants are typically dependent on the concentration difference between the compartments, the size of the fenestra, and the properties of the diffusing molecules [79]. The nanoparticles that enter the compartments after the bolus injection D_z at time $t_D \le t$ can be obtained by solving the rate equations

$$\begin{aligned} d_t a_1(t) &= -(k_{12}\,a_1(t) - k_{21}\,a_2(t)) - (k_{1n}\,a_1(t).....\\ &\quad .....- k_{n1}\,a_n(t)) - k_{10}a_1(t)\\ d_t a_2 &= k_{12}\,a_1 - k_{21}\,a_2\\ &\quad .\\ &\quad .\\ &\quad .\\ d_t a_n &= k_{1n}\,a_1 - k_{n1}\,a_n \end{aligned} \qquad (9)$$

with the initial conditions $a_1(0) = I(t_D)$, $a_2(0) = \ldots = a_n(0) = 0$, where $d_t = d/dt$ and $I(t_D) = D_z\delta(t)$.

Typically, nanoparticles' movement in and out of the compartments is through Brownian motion. Hence, the number of the nanoparticles in the compartments can be expressed as [42]

$$a_n(t) \sim Pois\,(\lambda(t)) \qquad (10)$$

where $Pois(.)$ is the non-homogeneous Poisson process with rate $\lambda(t)$. The solution to (9) can be obtained using numerical approach.

B. Nanocarriers' Anchoring at Targeted Sites

Where the nanoparticles that enter the targeted region are the nanocarriers, they bind to the targeted cells' surface receptors in a random manner by mean of high affinity ligand-receptor binding activities as shown in Fig.7. Typically, the surface receptors like the folate receptors are clustered on the cell surface [80]. Hence, assuming the same cell size and type, the number of clusters n_{Clu} on a cell surface multiplied by the number of cells n_{Cell} in a targeted site determines the number of anchorable points for the nanocarriers.

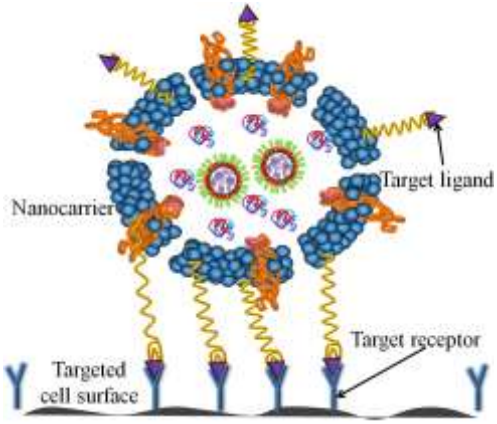

Fig. 7. Schematic illustration of nanocarrier anchoring at targeted site.

As the nanocarrier's surface and that of the targeted cell approach each other, the overall free energy of the system starts decreasing, and reaches a minimum at certain critical distance at which a bond is formed [81].

Implementation Issues: It was shown in [82] that the number of bonds that can be formed depends on the number of ligands on the nanocarrier's surface, the length of the tether, size of the nanocarrier, and receptor density on the surface of the targeted cells. The size of the nanocarrier and the length of the tether define the maximum area a nanocarrier can cover on the surface of the cell, which is termed area of influence (AOI) [81]. Hence, depending on the number and distribution of the receptors, one could design the nanocarrier to have optimum size, tether length and number of ligands to allow the carrier to form sufficient bonds with the receptors. Let n_L be the total number of ligands on a nanocarrier, and n_R the number of receptors in a cluster. It is then desirable that n_L/n_R is greater than unity to increase the chances of optimum ligand-receptor binding.

Let us assume that the size of nanocarrier and the length of the tether are chosen to obtain the optimum AOI, and that n_L/n_R is greater than unity. If we also assume that the optimal design is for the nanocarriers to anchor on one cluster, then the total number of nanocarriers A_{anc} that can anchor at a targeted site is

$$A_{anc} = n_{Clu} \times n_{Cell} \qquad (11)$$

where n_{Cell} is the number of cells that makes up a targeted site, and n_{Clu} is the number of clusters per cell.

V. Prodrug Release and Emission Characteristic

Recall from (5) that the emission characteristics of the Nano-T is defined by r_M, r_N, f_N, ∂_Ω, and $\wp$. Let us first consider the influence of $\wp$, which is related to the release mechanism of the liposomes inside the Nano-T, and defined by the activities in (1)-(4). After that, we shall present the emission model for the Nano-T taking into account r_M, r_N, f_N and ∂_Ω.

A. Release Mechanism

When the nanocarriers have anchored at the targeted sites, a trigger molecule of concentration $I(t)$ is injected into the body system, where they follow the same pharmacokinetic process as the nanocarriers to arrive at the targeted sites. We shall assume that on arriving at the sites, they are uniformly distributed across it. These trigger molecules bind to the molecules on the surface of the Nano-Ts and initiate the execution of the biochemical algorithm defined by (1)-(4). When a certain concentration of the PAA is cleaved through the biochemical activities in (1)-(4), the liposome stability is compromised, and the content release mechanism commences. Typically, the membrane stability is compromised by the cleaving of the linkers, which renders the headgroup less hydrophilic. As a result, the hitherto lamellar-alpha phase of the membrane lipids goes into the hexagonal II inverted phase, thereby releasing its contents [83]. The hexagonal II inverted phase is one of the polymorphism phases of lipid molecules in which they pack inversely to the packing observed in the orientation that allows the packing arrangement to encapsulated drug molecules.

The released prodrugs as a function of time can be expressed as [84]

$$v(t) = \alpha_0(1 - e^{-\gamma t}) \tag{12}$$

where γ is the release rate equivalent to the first-order rate constant, and α_0 is the cumulative concentration of the released drug molecules. Since we are interested in the specific concentration released at a given time instant, we can express this concentration as the density function given by

$$w(t) = d_t \alpha_0(1 - e^{-\gamma t}) \tag{13}$$

where $\alpha_0 = \int_0^T w(t)dt$, and T is the duration of the release.

By using the data in [52, Table 2] plotted in Fig. 8, we obtain the expression for γ, thus

$$\gamma = 0.3643 p_a - 0.1118 \tag{14}$$

where p_a is the concentration of the active protease. For p_a = 1, 1.5, 2 μM, the released molecular signal is shown in Fig. 9. It can be seen that the higher p_a is the faster the drug release.

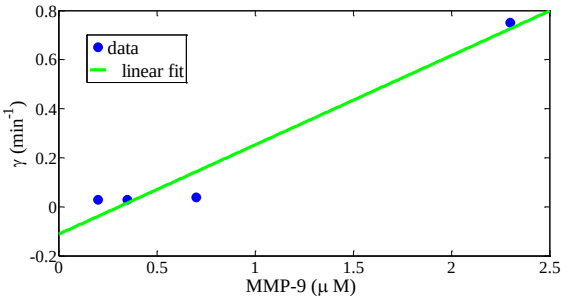

Fig. 8. Plot of γ versus release stimuli (MMP-9).

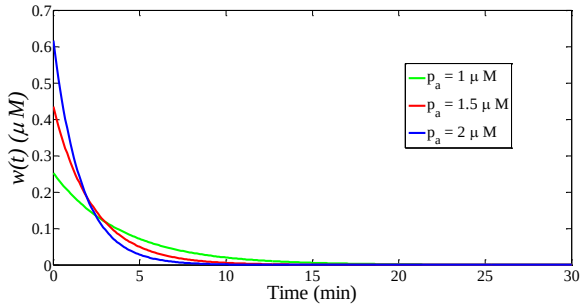

Fig. 9. Drug released by liposome as a function of release stimuli concentration.

B. Emission Model

While the release of the drugs from a liposome inside the Nano-T is defined by (13), the diffusion gradient-aided emission of the drug molecules is defined by r_M, r_N, f_N, and ∂_Ω. Earlier, we stated that the parameters r_M, r_N, f_N and ∂_Ω define the possibility of a diffusing molecules at an arbitrary time t being reflected back at some boundary points at the transmitter surface. Let us first assume that the drug releasing liposomes are not enclosed so that the influences of r_M, r_N, f_N and ∂_Ω are neglected. If $g_I(t,r)$ represents the concentration of the released prodrug at a reference surface that denotes an imaginary ∂_Ω depicted in Fig.10, then at time t and reference position r_0, the rate of change of g_I can be expressed as

$$d_t g_I(t, r_0) = w(t) + D d_{r_0 r_0} g_I(t, r_0) \quad ; r = r_0,\ 0 < t < \infty \tag{15}$$

where, $d_{r_0 r_0} = d^2 / dr_0^2$, and

$$d^2 / \partial r_0^2 = \frac{1}{r_0^2}\left(d_{r_0}\left(r_0^2 d_{r_0}\right) + \frac{1}{\sin\theta} d_\theta\left(\sin\theta\, d_\theta\right) + \frac{1}{\sin^2\theta} d_\phi^2 \right).$$

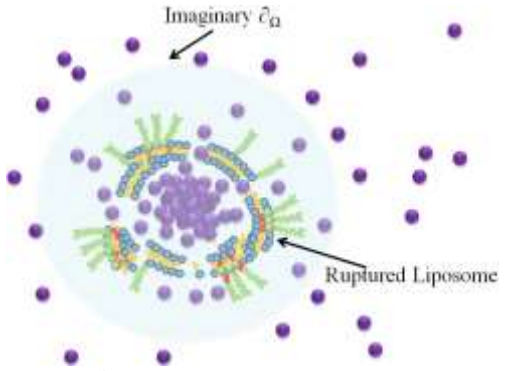

Fig. 10. Illustration of drug molecules emission observed at an imaginary surface ∂_Ω.

Let us consider the scenario where the propagation medium is homogeneous so that D is independent of (r,θ,ϕ). A solution to (15) can be obtained by modelling the source term $w(t)$ as a temporal distribution of released drug molecules such that

$$w(t) \approx w(l) = \sum_{i=0}^{L-1} h_l \delta(t + l\Delta\tau) \tag{16}$$

where h_l are the discretized concentrations at progressive steps $l\Delta\tau$ as is illustrated in Fig.11.

With (16) we can treat each sample of $w(l)$ as an impulsive release $h_l\delta(t+l\Delta\tau)$. Hence, we can modify (15) to become

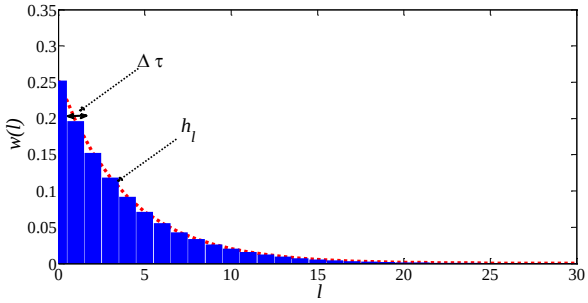

Fig. 11. Discretised release at progressive steps $l\Delta\tau$.

$$\begin{aligned} d_t g_I(t,r_0) &= D d_{r_0 r_0} g_I(t,r_0) \\ g_I(0,r_0) &= h_l \delta(t + l\Delta\tau) \\ g_I(t,0) &= 0 \end{aligned} \tag{17}$$

By solving (17) for each $h_l\delta(t+l\Delta\tau)$ and vectorially sum up the results, the concentration of the released drug molecules due to instantaneous loadings at $t+l\Delta\tau$ can be expressed as

$$g_I(t,r_0) = \sum_{l=0}^{L-1} \frac{h_l}{(4\pi D(t+l\Delta\tau))^{3/2}} e^{\frac{-(r_0)^2}{4D(t+l\Delta\tau)}} \tag{18}$$

where L is the number of samples considered.

Let us consider the case where there are K similar liposomes inside a given Nano-T with each encapsulating the same concentration of drug molecules. For K Liposomes that is randomly distributed inside the Nano-T, if they release their contents at approximately the same time, then

$$g_n(t,r_0) = \sum_{k=1}^{K} \sum_{l=0}^{L-1} \frac{h_{l,k}}{(4\pi D(t+l\Delta\tau))^{3/2}} e^{\frac{-(r_0-r_k)^2}{4D(t+l\Delta\tau)}} \tag{19}$$

where r_k, $k = 1, 2,..K$ is a randomly distributed variable, and $h_{l,k}$ is the h_l for the kth liposome. The expression in (19) is the total flux out of the imaginary surface ∂_Ω with respect to a given targeted site n.

Now, having obtain the expression for the emitted drug concentration without considering the effects of r_M , r_N, f_N and ∂_Ω, we shall proceed to add the influence of these parameters to (19) as is illustrated in Fig. 12. It is important that $r_M << r_N$ for the molecules to be able to diffuse easily through the pores. The expression for the diffusion coefficient that accounts for the ratio of the nanopore radius to that of diffusing molecules can be found in [85]. In this present work, we consider the case where $r_M << r_N$. Hence, we can relate the possibility of a diffusing molecule at an arbitrary time t being reflected back at some boundary points at the transmitter surface to the diffusion coefficient. Let P_d be the probability that a diffusing molecule at an arbitrary time t is reflected back. Thus

$$D_{eff} = \frac{K_B T}{6\pi\eta r_M} P_d\left(n_N, \frac{\partial_\Omega}{\partial_N}, f_N\right) \tag{20}$$

$$P_d(n_N) = 1 - \frac{1}{n_N} \; \mathcal{N}(\mu, \sigma^2) \tag{21}$$

where n_N is the number of the pores of equal dimensions, μ denotes the mean of the distribution, and σ^2 is the variance. As n_N tends to infinity, $D_{eff} = \frac{K_B T}{6\pi\eta r_M}$ [86], where K_B is the Boltzmann constant, T is the absolute temperature of the system, η is the viscosity of the diffusion medium and r_M is the radius of the spherically-shaped diffusing particle. Therefore, the expression (19) for the emitted drug concentration that take into account the effects of r_N, f_N and ∂_Ω, can then be written as

$$g_n(t,r_0) = \sum_{k=1}^{K} \sum_{l=0}^{L-1} \frac{h_{l,k}}{(4\pi D_{eff}(t+l\Delta\tau))^{3/2}} e^{\frac{-(r_0-r_k)^2}{4D_{eff}(t+l\Delta\tau)}} \tag{22}$$

For zero-mean unit variance, the effect of variation in n_N and invariably $\partial_\Omega/\partial_N$ is illustrated in Fig. 13 for $\alpha_0 = 10$, $r_0 = 1$, $\sigma^2 = 4$, $l = 1001$, and $\Delta\tau = 0.1$. It can be observed that D_{eff} produces a more noisy version of $g_n(t, r_0)$ as n_N value reduces. This noise can be regarded as a fluctuation in the concentration of the information molecules. Since it is this concentration that is detected by the receiver receptors (surface enzymes), implicitly, the random fluctuation (noise) in the information molecule concentration may result in deviations in the number of bound receptors/enzymes from the mean behavior predicted by deterministic models [87]. Hence, the lesser n_N is the more the effect of molecule random fluctuation is felt, and the more the deterministic model

assumption pursued in this work is violated. Note that if r_M is comparable to r_N, then the model will have to include the Knudsen diffusion [88] phenomenon.

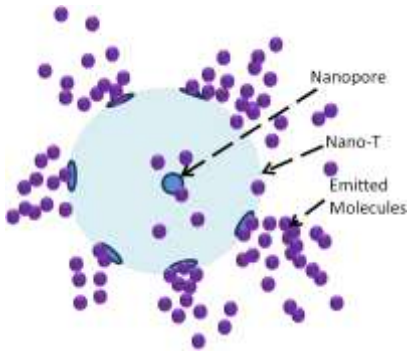

Fig. 12. Molecule emission through nanopores on the Nano-T membrane.

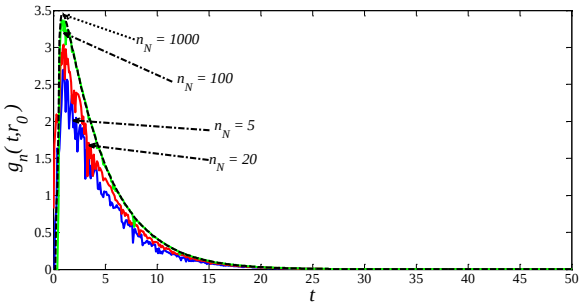

Fig. 13. Variation of $g_n(t, r_0)$ with n_N.

VI. Drug Reception Model at the Receiver-End

A. Emitted Drug Concentration Received in the Nano-R Reception Space

Let the Nano-R be located at a position r. The expression in (22) defines the input to the propagation channel, which is observed at a reference position $r_0 = r_R$. The expression for the concentration of the emitted drug molecules observed at a space around the receiver as shown in Fig.14 can be obtained by considering a radial solution to (17). The emitted drug is the concentration of the liposome-released drug observed at the immediate vicinity of the Nano-T membrane. To obtain the radial solution, let us assume that the distance between the Nano-T and the Nano-R is large enough so that we can consider the diffusing information molecules from the transmitter as being equally distributed around the Nano-R at time t. With this assumption, we can express the initial condition for (17) as the radial source

$$g_R(0,r) = \frac{h_l \delta(t + l\Delta\tau)}{4\pi r^2} \qquad g_R(t,0) = 0 \tag{23}$$

where r is the distance from the Nano-T to the center of Nano-R.

Following [89], the solution to (17) for the initial conditions (23), which accounts for the concept of the reception space, is expressed as contributions from each released $h_{l,k}$, thus

$$g_R(t,r) = \sum_{k=1}^{K}\sum_{l=0}^{L-1} \frac{h_{l,k}}{4\pi(r-r_k)r_{ass+}\left(4\pi D_{eff}(t+l\Delta\tau)\right)^{1/2}} \left\{ \exp\left(-\frac{\left|(r_{ass+} - (r-r_k))\right|^2}{4D_{eff}(t+l\Delta\tau)} \right) - \exp\left(-\frac{\left|(r_{ass+} + (r-r_k) - 2r_R)\right|^2}{4D_{eff}(t+l\Delta\tau)} \right) \right\} \tag{24}$$

where r_{ass+} is the radius of the reception space taken from the center of the spherical receiver. Hence, the concentration that is received in the reception space for $r_{ass+} \approx r_R$ can be obtained thus

$$\psi_n(t,r,r_R) = 4\pi r_R^2 D_{eff} d_r g_R(t,r)\Big|_{r_{ass+}=r_R} \tag{25}$$

The derivative in (25) can easily be obtained by differentiating the expression term-by-term. Hence,

$$\psi_n(t,r,r_R) = \sum_{k=1}^{K}\sum_{l=0}^{L-1} \frac{D_{eff} h_{l,k}(r_R(r-r_k) - r_R^2) e^{-\frac{(r_R-(r-r_k))^2}{4D_{eff}(t+l\Delta\tau)}}}{2\pi^{1/2}(D_{eff}(t+l\Delta\tau))^{3/2}(r-r_k)} \tag{26}$$

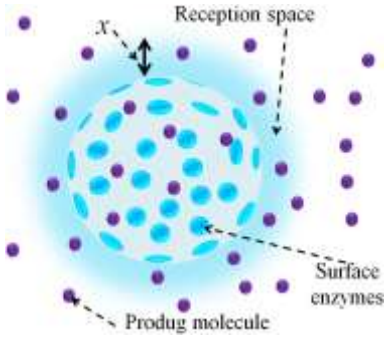

Fig. 14. An illustration of the reception space concept.

B. Activation of Received Inactive Drug Molecules

The molecular signal $\psi_n(t,r,r_R)$ is the concentration of the inactive drug that is available for activation by the immobilized enzymes on the surface of the Nano-R. By considering (8), we can model the activation of the prodrug molecules at the receiver by the following enzyme kinetics

$$d_t\psi_n(t,r,r_R) = -\xi_1\psi_n(t,r,r_R)q_0 + \xi_1\psi_n(t,r,r_R)c(t,r) + \xi_{-1}c(t,r) \tag{27}$$

$$d_t c(t,r) = \xi_1\psi_n(t,r,r_R)q_0 - \xi_1\psi_n(t,r,r_R)c(t,r) - \xi_{-1}c(t,r) - \xi_2 c(t,r) \tag{28}$$

$$d_t y_A(t,r) = \xi_2 c(t,r) \tag{29}$$

where $c(t,r)$ is the concentration of the prodrug-enzyme complex $Y_I E_R$, q_0 is the initial concentration of the enzyme E_R on the surface of the Nano-R, and $y_A(t,r)$ is the concentration of the active drug molecules Y_A.

The rate of formation of Y_A, is proportional to the rate at which Y_I and E_R encounter themselves, as well as the rate at which the encounter is broken. The rate of encounter is in

itself proportional to the joint probability of finding Y_I and E_R in the reception space at a given time. The rate at which the encounter is broken depends on the affinity constant ξ_a of the binding [90], which can be calculated as $\xi_a = \xi_1 / \xi_{-1}$. A high ξ_a implies that the received molecules stay long in the bonding; hence, more molecules may have diffused away within the bonding time t_{bond} and not get the opportunity to bond with the receptors. Recall, that we have assumed in the derivation of (26) that $r_{ass+} \approx r_R$, hence, the reception space $x = (r_{\text{ass+}} - r_{\text{R}})$ is very small. Let us expresses t_{d} as the observed time that a molecule of Y_I spends inside x, and $t_{bond} = t_{1/2} = 0.693/\xi_{-1}$ [90]. Then considering the scenario where $t_{\text{bond}} \leq t_{\text{d}}$, we can write that

$$\xi_{-1} \geq 1.386 D x^{-2} \tag{30}$$

This implies that the larger the value of reception space x, the higher the probability that many molecules may have diffused away from the space without getting the opportunity to bond with the receptors. In this case, a more accurate model must include the probability of escape from the space as a function of time. On the other hand, the smaller the value of reception space x, the lower the probability that some molecules may have diffused away from the space without getting the opportunity to bond with the receptors. In this case, a deterministic model can be pursued. In this case, the rate of complex formation will only depend on the concentration of surface enzymes $q(t)$ and Y_I at each point in time.

Assuming that $\psi_n(t,r,r_R) >> q(t)$, it can easily be shown that

$$y_A(t,r,r_R) = \frac{\xi_2 q_0 \psi_n(t,r,r_R)t}{\psi_n(t,r,r_R)+\xi_M} + \frac{e^{-[\xi_1\{\psi_n(t,r,r_R,t)+\xi_M\}]t+\log(\xi_1 q_0 \psi_n(t,r,r_R,t))}}{(\xi_1\{\psi_n(t,r,r_R)+\xi_M\})^2}$$

which is further reduced to

$$y_A(t,r,r_R) = \frac{\xi_2 q_0 \psi_n(t,r,r_R)t}{\psi_n(t,r,r_R)+\xi_M} + \frac{q_0 \psi_n(t,r,r_R,t) e^{-[\xi_1\{\psi_n(t,r,r_R,t)+\xi_M\}]t}}{\xi_1\{\psi_n(t,r,r_R)+\xi_M\}^2} \tag{31}$$

where $\xi_M = (\xi_{-1}+\xi_2)/\xi_1$ is the Michaelis-Menten constant. The proof of (31) is given in the Appendix.

C. Multiple-input Multiple-output Model of the Total Activated Drug Concentration at the Targeted Sites

In (31) the concentration of the activated drug with respect to one Nano-T and Nano-R configuration is given. However, since the number of communicating Nano-Ts and Nano-Rs in a site will likely be more than one, we need to develop the model for the multiple communicating nanodevices. In this work we present a model termed the distributed multiples input multiple output system for the diffusion-based MC in respect of TDD. The term distributed is used to imply that the input and output terminals are spatially displaced and do not cooperate with one another, which is the scenario in this case. We consider a two dimensional scenario where the targeted tissue can be approximately represented by a rectangular shape structure, with many nanoparticles anchoring on it. An illustration of this model is shown in Fig. 15, where T_{xi}, and R_{xj}, i,j =1,2… are the Nano-Ts and Nano-Rs, respectively, and g_{ij} is the impulse response of each transmit-receive link.

Let the anchor position of a nanocarrier be designated by the coordinate (x_i, ϕ_j). And let the anchor positions of the Nano-Ts and Nano-Rs be designated as, $(x_{i,T}, \phi_{j,T}) \in (x_i, \phi_j)$ and $(x_{i,R}, \phi_{j,R}) \in (x_i, \phi_j)$. The transmit-receive distance between a Nano-T and a Nano-R can be expressed as

$$\varsigma_\nu = \sqrt{(x_{i,R}-x_{i,T})^2 + (\phi_{j,R}-\phi_{j,T})^2}; \quad \nu = 1,2,..,M_T \times M_R \tag{32}$$

where M_T and M_R are the numbers of the Nano-T and Nano-R that anchor on a tissue.

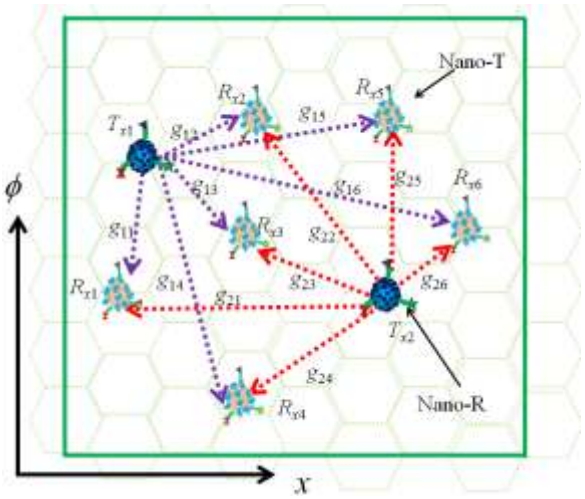

Fig. 15. Distributed MIMO configuration for MC-based TDD system for M_T = 2 and M_R = 6.

Let us first neglect the presence of all the Nano-Rs but one. The combined concentration of drug from all the Nano-Ts, activated by a single Nano-R can be expressed by

$$y_{A,T}(t,\varsigma_\nu,r_R) = \sum_{\nu=1}^{M_T} \frac{\xi_2 q_0 \psi_{T,n}(t,\varsigma_\nu,r_R)t}{\psi_{T,n}(t,\varsigma_\nu,r_R)+\xi_M} + \frac{q_0 \psi_{T,n}(t,\varsigma_\nu,r_R) e^{-[\xi_1\{\psi_{T,n}(t,\varsigma_\nu,r_R,t)+\xi_M\}]t}}{\xi_1(\psi_{T,n}(t,\varsigma_\nu,r_R)+\xi_M)^2} \tag{33}$$

where $\nu = 1,2,..,M_R \times 1$ is the contributions from all the M_T Nano-Ts dispersed on the targeted tissue's surface.

Now, if we take all the Nano-Rs into account, then the derivation of (33) should take into account the fact that at each Nano-R, molecules (inactive drugs) are catalyzed into a new

molecule (active drugs), thereby creating a loss in the overall concentration of the inactive drug molecules. This loss can be stochastically modeled based on capture-and-extract mechanism where the molecules that are deemed received are removed from the system. Another approach will be to include a reaction term in (17) and derive (33) with respect to a reaction diffusion equation. Implicitly, (17) will become

$$d_t g_I(r_0,t) = D d_{r_0 r_0} g_I(r,t) - R_k g_I(r,t) \tag{34}$$

which is a reaction-diffusion equation, where R_k is the rate of reaction; a function of the surface enzyme concentration.

If however, the total concentration of the inactive molecules propagating in the medium is far greater than that of the surface enzymes, then it implies that the second term on the right-hand-side of (34) is negligible. And assuming that molecules that are emitted from the Nano-Ts do not re-enter any of the Nano-Ts, then the concentration of the drugs activated by the *j*th Nano-R can be approximated by

$$\begin{aligned} y_{T,n,j}(t,\varsigma_\nu,r_R) \approx & \sum_{\nu=1}^{M_T} \frac{\xi_2 q_0 \psi_{T,n}(t,\varsigma_\nu,r_R) t}{\psi_{T,n}(t,\varsigma_\nu,r_R)+\xi_M} \\ & + \frac{q_0 \psi_{T,n}(t,\varsigma_\nu,r_R) e^{-[\xi_1\{\psi_{T,n}(t,\varsigma_\nu,r_R)+\xi_M\}]t}}{\xi_1(\psi_{T,n}(t,\varsigma_\nu,r_R)+\xi_M)^2} + n_y(t) \end{aligned} \tag{35}$$

where $\nu = 1,2,..,M_T \times 1$ and $n_y(t) \sim \mathcal{N}(\mu, \sigma^2)$ with mean μ and variance σ^2 is the noise term that accounts for the randomness with which molecules diffuse to even out the captured-and-extracted drug (activated drug) molecules. Hence, the total concentration of the activated drug molecules at a given targeted site *n* is given by

$$y_{T,n}(t,r,r_R) = \sum_{j=1}^{M_R} y_{T,n,j}(t,\varsigma_\nu,r_R) \tag{36}$$

VII. Nanoparticles' Injection Sequence and Timing Optimization

In this work, we have considered a bolus injection approach for all the nanoparticles. Let t_A, t_B and t_C , $\{t_A, t_B, t_C\} \in t_D$ represent the times at which the Nano-T, Nano-R and trigger molecules, respectively, are injected into the body system. If $t_C < \{t_A, t_B\}$, then the Nano-Ts release and Nano-Rs activation mechanisms will be triggered in the blood system, thereby intoxicating the entire system, which is not the desired goal of TDD. Hence, it is important that $t_C > \{t_A, t_B\}$ is ensured to achieve good results. And it is also necessary that a significant time period between $\{t_A, t_B\}$ and t_C, $t_C > \{t_A, t_B\}$ is observed so as to ensure that many of the nanocarriers have lodged in the targeted sites with insignificant number in the blood system.

The sequence of injecting the nanocarriers is also crucial. It is essential that nanocarriers are injected in a sequence that guarantees that the approximate desired numbers of the difference carriers locate and anchor at the targeted sites. If we inject one type of nanocarrier before the other, there is a significant probability that one or more of the targeted sites may have many of its anchor location fully occupied leaving no space for the subsequently injected nanocarriers to anchor. If however, both are introduced at the same time and in well-mixed concentration, there is an equal chance for each type of nanocarrier to find its way into the targeted sited. In this work, we suggest that to achieve efficient drug delivery the optimal injection approach is to ensure that the following conditions hold; $t_C > \{t_A, t_B\}$, the difference between t_C and $\{t_A, t_B\}$is large, $t_A = t_B$ is observed, and the mixture of Nano-Ts and Nano-Rs is homogeneous.

Hence, we can quantify the injection sequence and timing performance by the number of nanocarriers N_{REM} present in the blood system (compartment 1) at the time t_{Tin} of injecting the trigger molecules into the system.

VIII. Numerical Results and Discussion

The main objective of any TDD system is to deliver the right concentration (dose) of a therapeutic drug to targeted sites in the body in such a manner that other non-targeted sites are minimally affected. Based on the discussions in this work, the effectiveness of the proposed multiple site TDD system to achieving the above objective primarily depends on 1) the capacity and release/emission efficiency of the Nano-Ts, 2) the reception capability of the Nano-Rs, 3) the efficiency with which the trigger molecules excite the Nano-Rs, 4) the number of the nanocarriers, 5) the ability of the nanocarriers to establish a stable bond at the targeted site and, 6) the number of Nano-Rs that are left out from the targets site, but still circulating in the blood system.

In this section, we carry out the evaluation of the proposed MC-based TDD model in terms of its effectiveness. Specifically, we consider the effects of the parameters associated with the Nano-T and Nano-R design, the diffusion characteristic of the targeted sites, and the timing of the injection of the nanoparticles. Firstly, we create a scenario for the simulation. Secondly, calculation example in terms of the drug encapsulation capacity of the Nano-T is presented. Thirdly, the parametric design of the Nano-R is discussed. Fourthly, the method for simulating the pharmacokinetic model is presented. Finally, simulation results are presented with respect to the effect of the nanocarriers' parameters and diffusion coefficient on the concentration of the potent drug delivered.

A. Simulation Scenario and Targeted Sites

The scenario of interest here is the one depicted in Fig. 1 and is illustrated further in Fig.16. In Fig.16, the human body or environment is modeled as containing two targeted tissue sites, Site 1 and Site 2. A number of Nano-Ts and Nano-Rs are injected into the blood system. These nanocarriers diffuse passively through the blood system until they arrive at the targeted sites. At the targeted sites, they bind to the intrinsically expressed receptors on the surfaces of the tissues using their corresponding complementary target ligands

tethered on their membranes. Subsequently, the appropriate trigger molecules are injected into the blood network. The trigger molecules also diffuse passively until they encounter and bind to the receptors on the surface of the Nano-Ts. At that point, the communication process, as well as the drug delivery operation, commences.

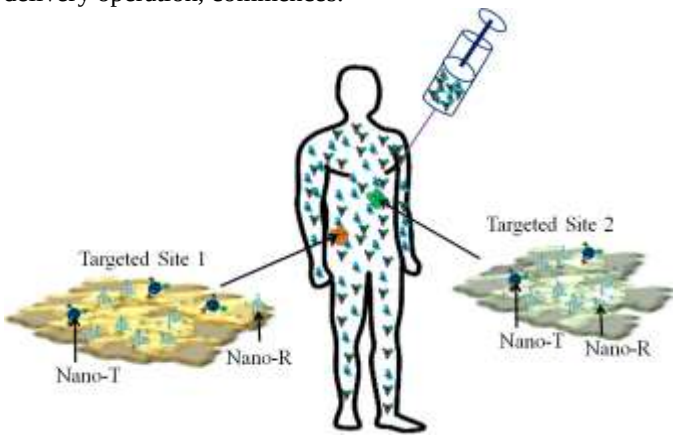

Fig. 16. Illustrative scenario for the MC-based multiple site TDD. *This diagram is best viewed in color*.

In this simulation, the dimensions of Site 1 and 2 are taken to be 200 × 200 μm^2 each, and are composed of cells of size 20 μm. For simplicity, we assume that the inter cluster spacing is 10 μm, which gives us a maximum of two clusters per cell surface. Hence, assuming that one nanocarrier can anchor only on one cluster, the total numbers of anchorable points A_{anch} on each site surfaces is 200. The diffusion coefficient D of each of the targeted site medium is taken to be 0.85 mPa s^{-1} [11].

B. Nano-T Parametric Design

The capacity of the Nano-T is defined here as the amount of drug molecules it can hold. This depends on its size and the size/number of the drug encapsulating liposomes enclosed in the Nano-T's interior. In choosing the size of the Nano-T (as well as the Nano-R), we consider two factors; the size of the associated fenestrae that will facilitate the passage of the carriers into the targeted sites, and the nanocarrier size that will minimize the probability of the nanocarrier being phagocytized. Large-sized nanoparticles are known to be easily removed from the system by microphages [90, 91]. This puts a limit to how large we can go with size. More also, the bigger the size, the less possible it is to pass through narrow blood vessels and eventually the fenestrae into the ECM to reach the targeted sites.

The smallest vessel, the capillary, has the diameter of 5-10 μm [92] and the fenestrae on the endothelia for a tumor cells is about 240-400 nm [93, 94]. Hence, we can choose the radius r_{T} of the spherical Nano-T to be between 0.1 and 0.2 μm. Its volumetric capacity can be calculated by $V_{\text{T}} = (4/3)\pi r_{\text{T}}^3$. To make allowance for the volume occupancy of fluids and the protease, the inner radius of the enclosed liposome is given as $r_{\text{L}} = r_{\text{T}}/2$. In this simulation we consider only one enclosed liposome, that is, $K = 1$. Hence, the encapsulated drug per liposome is $V_{\text{encap}} = (1/6)\pi r_{\text{T}}^3$. The encapsulated prodrug concentration for $r_{\text{T}} = 0.18$ μm nm is 3.054×10^{-3} μm^{-3}. Let us assume that Site 1 and Site 2 require 1μL and 0.6 μL of drugs for effective therapy, respectively. Hence, we can speculate that about 3.28×10^{11} and 1.97×10^{11} Nano-Ts are required in Site 1 and 2, respectively. This implies that a conventional 10ml syringe has the capacity of injecting about 3.28×10^{12} Nano-Ts in a single shot. The transmitter capacity versus r_{T} is plotted in Fig. 17 for different r_{T} to r_{L} ratios. It can be seen that the higher the ratio, the more the capacity. This increase is at the expense of a faster release rate since this implies smaller concentration of the p_a to facilitate faster release (see Fig.8 and 9).

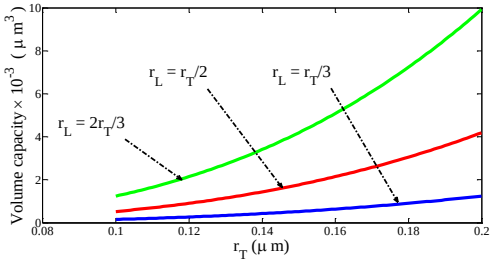

Fig. 17. Volume capacity as a function of the Nano-T radius and the ratio of r_{T} to r_{L}.

On the other hand, the emission capability of the Nano-T depends on rate of release and the number of nanopores. Hence, the concentration of p_a should be kept high enough to ensure fast release. In the simulation, for reasons pointed out in Section V, we keep the ratio of the nanopores footprint to the Nano-T's surface area at value that tends to unity. In this sense, n_N =100000 is chosen for all the simulations in this section.

B. Nano-R Parametric Design

The vital Nano-R parameters are size and the concentration of the surface enzymes. A large surface area allows for more enzymes and tethered ligands to be incorporated. The more the tethered ligands is, the higher the probability of the Nano-R to form a bond on the surface of the targeted tissue as was discussed in Section IV. And the more the surface area of the Nano-R the more enzymes are incorporated thereby increasing the number of prodrug molecules activated per unit time. However, like in the case of the Nano-T, there is a limit to how large the Nano-R can be so as to allow it to pass through the fenestrae into the ECM, and not to be phagocytized. We limit the radius of the Nano-Rs to less than or equal to 0.180 μm, which is half the maximum dimension of a fenestrae on the endothelia for tumor cells. Subsequently, we will examine the effect of the receiver size on the performance of the proposed TDD system. Specifically, we relate the r_R to the effective enzyme concentration $e_{\text{eff,R}}$ defined by the expression [11]

$$e_{\text{eff,R}} = b n_E \rho \qquad (37)$$

where $\rho = r_R^2 / r_E^2$, r_E is the enzyme base radius, n_E is the molar mass of the enzyme and b is termed *active enzyme factor*. The plot of the effective enzyme concentration is shown in Fig. 18. It can be seen that as the r_R gets bigger, the enzyme concentration increases expectedly, and the variation between one active enzyme factor and another increases as well. Hence, one can adjust the concentration of the activated drug by varying either the radius of the Nano-R or the active enzyme factor.

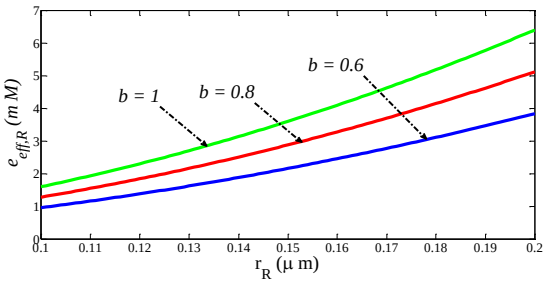

Fig. 18. Variation of effective enzyme concentration with r_R and b.

In our simulations, the following the following Nano-R parameter values are used, r_E = 0.005 μm and n_E = 4 μM. Instead of the value of b = 1 used in [11], we choose b = 0.6 to account for the spaces on the Nano-R's surface where the target ligands are tethered.

C. Nanocarriers' Pharmacokinetics Simulation

For a bolus injection of a dose D_z of the well-mixed concentration of the Nano-T and Nano-R, we consider a three-compartment model comprising of the blood system and two targeted sites. The resulting first-order ordinary differential equations are solved numerically. From [96], which presented the application of pharmacokinetic to the development of liposomal formulations for oncology, the values of k_{10}, k_{12} and k_{21} used in this paper are obtained. The values of k_{10}, k_{12} and k_{21} used are 0.0082 min^{-1}, 0.047 min^{-1}, 0.00125 min^{-1}, respectively, for compartment 2. For compartment 3, the values k_{13} = 0.0367 min^{-1}and k_{31} = 0.0124 min^{-1} used in [97] to determine the pharmacokinetics of Remifentanil are employed in this work.

In Fig.19, the result of the numerical evaluation of the pharmacokinetic model in (9) is compared to Monte Carlo results. In Fig.19, D_z = 10 is used, and λ is varied between 0.1 and 1. It can be seen that there is a good agreement between the (9) and the Monte Carlo simulation.

Now, let us consider the scenarios where t_{Tin} values are 10, 30 and 60 mins for D_z = 400. It is important that the release takes place only at the targeted sites, hence, we have earlier set the condition $t_{Tin} = t_C > \{t_A, t_B\}$ to ensure that minimal release takes place in the blood compartment. The success of this minimization approach is quantified by the number of the nanocarriers N_{REM} that are still circulating in the compartment 1 at the time of injecting the trigger molecule. Table I shows the N_{REM} for varying values of the rate constants k_{12} and k_{13}, which represent the rates at which the nanocarriers enter the targeted sites. As mentioned earlier, these constants are dependent on the size of the fenestrae. Hence, if we modify the sizes of the nanocarriers to obtain high rate constants without compromising capacity and reception efficiency, we will be able to reduce N_{REM} significantly, and minimize the possibility of drug release in the blood compartment.

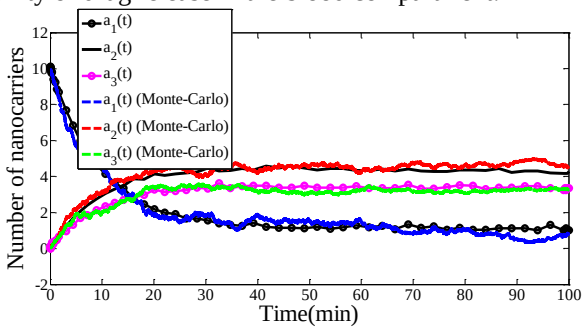

Fig. 19. Nanocarrier amount for compartments 1, 2 and 3 as a function of time.

TABLE I
VARIATION OF N_{REM} WITH k_{12} AND k_{13}

Rate constants	k_{12} = 0.0475; k_{13} = 0.0367		
	t_{Tin} = 10 min	t_{Tin} = 30 min	t_{Tin} = 60 min
N_{REM}	168	59	42
Rate constants	k_{12} = 0.1475; k_{13} = 0.1367		
	t_{Tin} = 10 min	t_{Tin} = 30 min	t_{Tin} = 60 min
N_{REM}	35	16	15
Rate constants	k_{12} = 0.475; k_{13} = 0.367		
	t_{Tin} = 10 min	t_{Tin} = 30 min	t_{Tin} = 60 min
N_{REM}	6	5	5

TABLE II
VARIATION OF N_{REM} WITH k_{10}

Rate constants	k_{10} = 0.0082		
	t_{Tin} = 10 min	t_{Tin} = 30 min	t_{Tin} = 60 min
N_{REM}	168	59	42
Rate constants	k_{10} = 0.082		
	t_{Tin} = 10 min	t_{Tin} = 30 min	t_{Tin} = 60 min
N_{REM}	86	15	10
Rate constants	k_{10} = 0.82		
	t_{Tin} = 10 min	t_{Tin} = 30 min	t_{Tin} = 60 min
N_{REM}	0	0	0

In Table II, we show the N_{REM} for different values of the elimination rate constants k_{10}, which represent the rates at which the nanocarriers are removed from the blood compartment by the process of phagocytosis. It can be seen in Table II that higher values of k_{10} reduces N_{REM} significantly, and minimize the possibility of drug release in the blood compartment. And as discussed earlier, the larger the nanocarriers, the more likely they will undergo phagocytosis, hence, higher k_{10}. But going for higher k_{10} implies increasing size which will undesirably reduce k_{12} and k_{13}. Hence, an

optimal size that ensures balance among the rate constants must be sought after.

D. Distributions of Anchored Nanocarriers on the Sites

Let a_2 and a_3 be the number of the nanocarriers that accumulated at the targeted sites 1 and 2. Note that a_2 and a_3 include the number of the Nano-Ts and Nano-Rs. Since they are well-mixed in the originally injected dose, each has the probability of diffusing into targeted site that is approximately proportional to their number in the injected dose. Hence, if a_{IT} and a_{IR} are the initial numbers of the Nano-T and Nano-R in the injected dose, then

$$a_{T,tar,n} = \frac{a_{IT}}{D_z} \times a_n \tag{38}$$

$$a_{R,tar,n} = \frac{a_{IR}}{D_z} \times a_n \tag{39}$$

where $a_{T,tar,n}$ and $a_{R,tar,n}$, n = 1, 2 are the numbers of the Nano-Ts and Nano-Rs delivered to each site n.

For the given dimension of the targeted site with maximum anchorable points A_{anch}, we randomly locate the nanocarriers on the cluster positions noting that A_{anch} is greater or equal to the total number of nanocarriers.

We can adapt Table I to the discussion here to give the concentration of the drug that is available for release in the blood compartment. Let us consider the ratio of Nano-T to Nano-R at the time of the injection to be 1:10 and 3:8, where the volume capacity of the Nano-T is 3.054 × 10^{-3} μm^{-3}. By using (38) and (39), the concentrations of the drug that is releasable in the blood compartment for different t_{Tin} and rate constants are shown in Table III. This give a clearer picture of the level of toxicity that is associated with the various rate constants. In Table III, it can be seen that higher rate constant gives lower toxicity, a statement that is in agreement with Table I.

TABLE III
DRUG CONCENTRATION RELEASABLE IN THE BLOOD COMPARTMENT FOR DIFFERENT VALUES OF t_{Tin}, k_{12} AND k_{13}

Rate constants	k_{12} = 0.0475; k_{13} = 0.0367		
	t_{Tin} = 10 min	t_{Tin} = 30 min	t_{Tin} = 60 min
Conc. (10^{-3} μm^{-3}) @ 1:10	46.64	16.38	11.66
Conc. (10^{-3} μm^{-3}) @ 3:8	139.93	49.14	34.98
Rate constants	k_{12} = 0.1475; k_{13} = 0.1367		
	t_{Tin} = 10 min	t_{Tin} = 30 min	t_{Tin} = 60 min
Conc. (10^{-3} μm^{-3}) @ 1:10	9.72	4.44	4.16
Conc. (10^{-3} μm^{-3}) @ 3:8	29.15	13.33	12.49
Rate constants	k_{12} = 0.475; k_{13} = 0.367		
	t_{Tin} = 10 min	t_{Tin} = 30 min	t_{Tin} = 60 min
Conc. (10^{-3} μm^{-3}) @ 1:10	1.67	1.39	1.39
Conc. (10^{-3} μm^{-3}) @ 3:8	5.00	4.17	4.17

E. Simulations for the Activated Drugs at Targeted Sites

With the nanocarriers in positions at the targeted sites and the trigger molecules injected, the reaction sequence (1)-(4) executes to release the prodrug molecules. We assume that the average value of the activated protease is p_a = 1 μM, hence, γ = 0.26 min^{-1}. Let us assume that the target dose for this simulation is 3.054 × 10^{-2} μm^{-3} for both sites. Since, the capacity of the Nano-T with r_{T} = 0.18 μm is about 3.054 × 10^{-3} μm^{-3}, we will require at least 10 Nano-Ts. We shall consider the following Nano-T to Nano-R ratios; 1:10, 1:15, and 1:20 for both targeted sites. Hence, for D_z = 400, the pharmacokinetics output gives a_2 = 173 and a_3 = 135. By using (38) and (39), the ratio 1:10 yield $a_{\text{T,tar},1}$ = 15, $a_{\text{T,tar},2}$ = 12, $a_{\text{R,tar},1}$ = 173 - $a_{\text{T,tar},1}$, $a_{\text{T,tar},2}$ = 135 - $a_{\text{T,tar},2}$; the ratio 1:15 yield $a_{\text{T,tar},1}$ = 10, $a_{\text{T,tar},2}$ = 8, $a_{\text{R,tar},1}$ =173 - $a_{\text{T,tar},1}$, $a_{\text{T,tar},2}$ =135 - $a_{\text{T,tar},2}$; and the ratio 1:20 yield $a_{\text{T,tar},1}$ = 8, $a_{\text{T,tar},2}$ = 6, $a_{\text{R,tar},1}$ =173 - $a_{\text{T,tar},1}$, $a_{\text{T,tar},2}$ =135 - $a_{\text{T,tar},2}$. For the following kinetic constants $\xi_1 = 50$, $\xi_2 = 8$, $\xi_M = 0.1$, the total normalized drug concentration activated at Site 1 and Site 2 for the different Nano-T to Nano-R ratios are shown in Fig. 20 and 21.

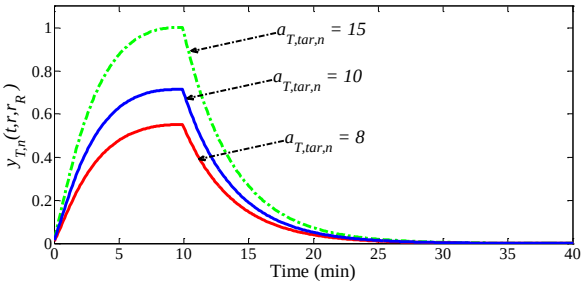

Fig. 20. Variation in the total normalized drug concentration activated at Site 1 for different number of Nano-Ts and the same number of Nano-Rs.

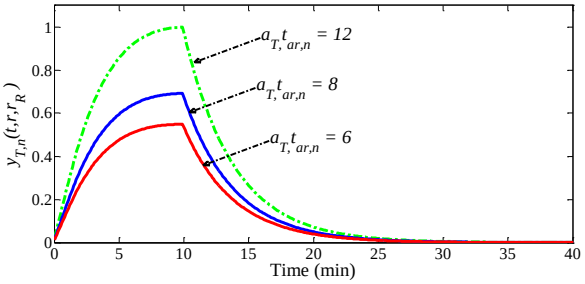

Fig. 21. Variation in the total normalized drug concentration activated at Site 2 for different number of Nano-Ts and the same number of Nano-Rs.

Fig. 20 and 21 show as envisaged that the more the number the Nano-Ts, the more the drug concentration that is delivered. However, as can be inferred from Table III, higher number of Nano-Ts also implies increase in the possible number of Nano-Ts that can release drugs unwantedly in the blood compartment.

To investigate the effect of the Nano-R parameters, we vary the radius r_{R}, in accordance with (37). The plot of the total normalized activated drug concentration is shown in Fig. 22 for different receiver radii. Fig. 22 indicates that larger receiver radius results in higher concentration of the activated drug molecules. However, impediments such as the dependency of unwanted drug delivery in the blood

compartment, and the possibility of phagocytosis on the Nano-T size, limit how high we can go with nanocarrier size.

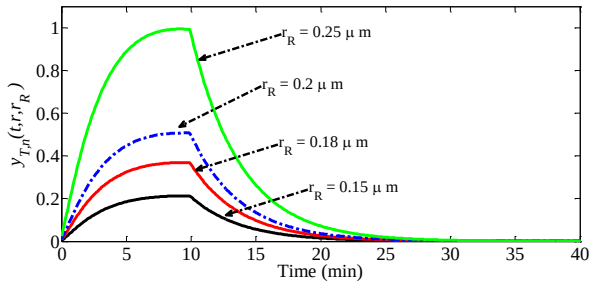

Fig. 22. Variation in the total normalized drug concentration activated at Site 1 for different receiver radius.

The time dispersive characteristics of the drug molecules distribution at the targeted sites are illustrated in Fig. 23. It can be observed that as time progresses, and depending on the concentration, more drugs tend to diffuse into adjacent cells. Hence, the delivered concentration should be kept as close as possible at the minimal dose level to reduce the possibility of

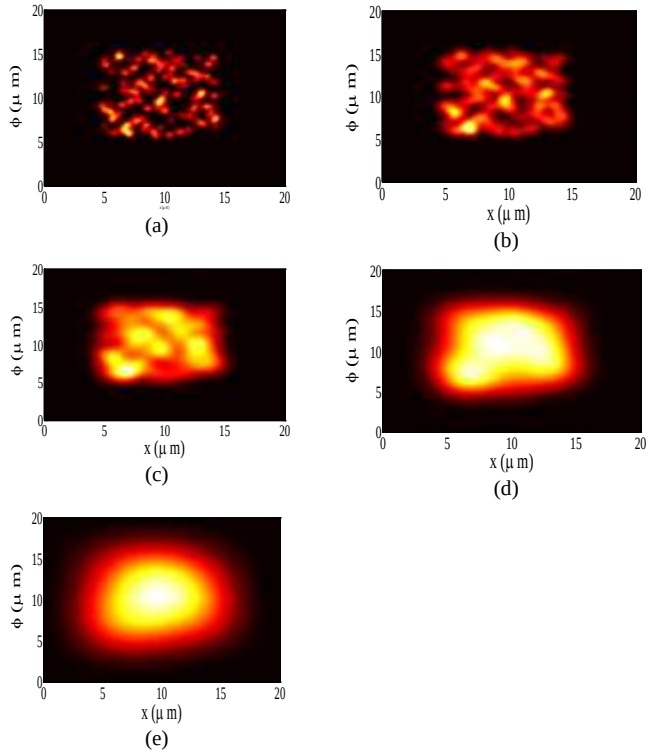

Fig. 23. Distribution of the delivered active drug at Site 1 as a function of time (a) 0.0001 min (b) 0.001min (c) 0.01min (d) 0.1min (e) 1 min. *This diagram is best viewed in color*.

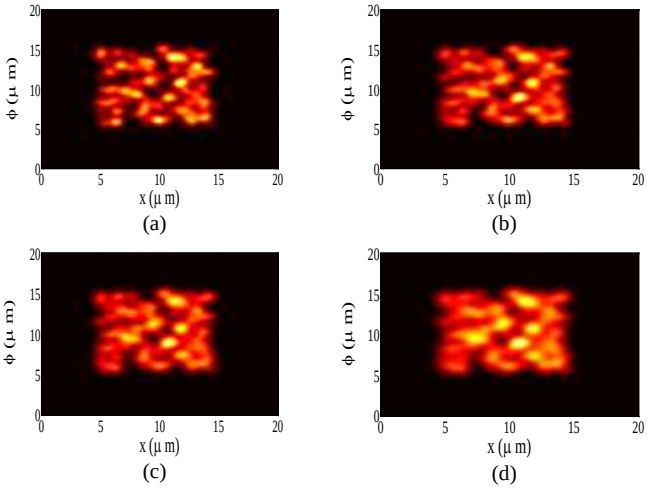

Fig. 24. Distribution of the delivered active drug at Site 1 as a function of the diffusion coefficient of the medium D = (a) 0.6 (b) 0.8 (c) 1.0 (d) 2.0, at t = 0.001 min. *This diagram is best viewed in color*.

adjacent cells being affected. The influence of the diffusion characteristics of the tissue medium on the rate of dispersion of the delivered drug is shown in Fig. 24. It can be observed that the higher the diffusion coefficient the more the drug molecules disperse in time. Hence, for a higher diffusion coefficient delivered drug molecules will disperse more quickly and tend to move undesirably into the adjacent cells than for lower diffusion coefficient.

IX. Conclusion

In this paper, we have presented an MC-based enzyme-triggered liposome-dependent TDD model for therapeutic actions in multiple targeted sites where release stimuli are not expressed. The proposed model incorporated self-trigger techniques that are not dependent on the stimuli present at the targeted sites. To avoid delivering potent drugs to non-target sites due to unforeseen catastrophic failure, prodrugs that can be activated at the target sites have been used instead of potent drugs. We have also provided analytical expressions for the various input and output molecular signals of the model. The effectiveness of the proposed model in terms of the transmitter volume capacity and radius, the receiver radius, and the diffusion characteristics of the site medium was also evaluated.

Although the focus of this work is on drug delivery, the proposed system can also be used to deliver other forms of information molecules to the body and other systems of interest. For instance, with little reconfiguration, it can be used to deliver antibodies, DNA and nano imaging particles to targeted sites.

APPENDIX

The proof of (31) is presented here. Assuming that $\psi_n(t,r,r_R) >> q(t)$, (28) simplifies to a pseudo first-order equation, where

$$\int \frac{dc(t,r)}{\xi_1\psi_n(t,r,r_R)q_0 - [\xi_1\psi_n(t,r,r_R)+\xi_{-1}+\xi_2]c(t,r)} = \int dt \qquad \text{(A1)}$$

Integrating both sides of (A1) yields

$$\frac{\log_e [\xi_1\psi_n(t,r,r_R)q_0 - [\xi_1\psi_n(t,r,r_R)+\xi_{-1}+\xi_2]c(t,r)]}{-[\xi_1\psi_n(t,r,r_R)+\xi_{-1}+\xi_2]} = t+\vartheta \qquad \text{(A2)}$$

For the initial consition $c(t=0,r)=0$,

$$\vartheta = \frac{\log_e[\xi_1\psi_n(t,r,r_R)q_0]}{-[\xi_1\psi_n(t,r,r_R)+\xi_{-1}+\xi_2]} \qquad \text{(A3)}$$

Hence

$$c(t,r) = \frac{\psi_n(t,r,r_R)q_0}{[\psi_n(t,r,r_R)+\xi_M]} - \frac{e^{-[\xi_1\psi_n(t,r,r_R)+\xi_{-1}+\xi_2]t+\log(\xi_1 q_0\psi_n(t,r,r_R))})}{[\psi_n(t,r,r_R)+\xi_M]\xi_1} \qquad \text{(A4)}$$

where $\xi_M = (\xi_{-1}+\xi_2)/\xi_1$ is the classical Michaelis-Menten kinetic constant.

Plugging (A4) into (29), we obtain

$$y_A(t,r) = \int \xi_2 c(t,r)\, dt \qquad \text{(A5)}$$

Solving (A5) as a pseudo first-order equation yields (31)

$$y_A(t,r,r_R) = y_A(t,r) = \xi_2\left(\frac{\psi_n(t,r,r_R)q_0}{[\psi_n(t,r,r_R)+\xi_M]}t + \frac{e^{-[\xi_1\psi_n(t,r,r_R)+\xi_{-1}+\xi_2]t+\log(\xi_1 q_0\psi_n(t,r,r_R))}}{([\psi_n(t,r,r_R)+\xi_M]\xi_1)^2}\right) \qquad \text{(A6)}$$

REFERENCES

[1] R. A. Freitas, "Current status of nanomedicine and medical nanorobotics," *J Comp. and Theo. Nanosc.*, vol. 2, no.1, 2005 pp. 1-25.

[2] D. K. Kim, and J Dobson, "Nanomedicine for targeted drug delivery," Journal of Materials Chemistry 19, no. 35 (2009): 6294-6307.

[3] I. Akyildiz, F. Brunetti, and C. Blázquez, "Nanonetworks: a new communication paradigm," *Computer Networks*, vol. 52, no. 12, pp. 2260-2279, 2008.

[4] L. G. Griffith and G. Naughton, "Tissue engineering – current challenges and expanding opportunities," *Science*, vol. 295, no. 5557, pp. 1009–1014, 2002.

[5] J. Clausen, "Man, machine and in between," *Nature*, pp. 1080–1081, 2009.

[6] M. T. Barros, S. Balasubramaniam, and B. Jennings, "Using information metrics and molecular communication to detect cellular tissue deformation," *IEEE Trans. Nanobioscience*, vol. 13, no. 3, 2014, pp.

[7] R. A. Freitas, "Current status of nanomedicine and medical nanorobotics," *J Comp. and Theo. Nanosc.*, vol. 2, no. 1, pp. 1-25, 2005.

[8] Y. Chen, P. Kosmas, P. Anwar, and L Huang, "A touch-communication framework for drug delivery based on a transient microbot system," *IEEE Trans. Nanobioscience*, vol. 14, no. 4, 2015, pp. 397-408.

[9] B. Atakan, O. B. Akan, and S. Balasubramaniam, "Body area nanonetworks with molecular communications in nanomedicine," *IEEE Communications Magazine*, vol. 50, no. 1, 2012, pp. 28-34.

[10] Y. Chahibi, M. Pierobon, S. O. Song, and I. F. Akyildiz, "A molecular communication system model for particulate drug delivery systems," *IEEE Trans. Biomed Eng*, vol.60, no.12, pp.3468-3483, 2013.

[11] U. A. K. Chude-Okonkwo, "Diffusion-controlled enzyme-catalyzed molecular communication systems for targeted drug delivery," *IEEE Global Communication* Conference, Austin, Texas, Dec. 8-12, 2014.

[12] D. Malak, and O. B. Akan, "Molecular communication nanonetworks inside human body," *Nano Communication Networks*, vol. 3, no. 1, 2012, pp. 19-35.

[13] R. Byrne and D. Diamond, "Chemo/bio-sensor networks," *NatureMaterials*, vol. 5, pp. 421– 424, 2006.

[14] N. Kumar, *Handbook of Particulate Drug Delivery (Nanotechnology book Series) vol. 1*, American Scientific Publishers, CA, USA, 2008.

[15] P. Debbage, "Targeted drugs and nanomedicine: present and future," *Current pharmaceutical design*, vol. 15, no. 2, 2009, pp. 153-172.

[16] M. A, Firer and G. Gellerman, "Targeted drug delivery for cancer therapy: the other side of antibodies," *J Hematol Oncol*, vol. 5, no. 1, 70, 2012.

[17] C. F. Greineder, et al., "Advanced drug delivery systems for antithrombotic agents," *Blood*, vol. 122, no.9, 2013, pp. 1565-1575.

[18] Y. Yeo, (ed.), *Nanoparticulate drug delivery systems: strategies, technologies, and applications*, New Jersey: John Wiley & Sons, 2013.

[19] G. Sharma, S. Anabousi, C. Ehrhardt, and M. N. V. Ravi Kumar, "Liposomes as targeted drug delivery systems in the treatment of breast cancer," *Journal of drug targeting*, vol. 14, no. 5, 2006, pp. 301-310.

[20] J. ElHazzat and M. E. H. El-sayed, "Advances in targeted breast cancer therapy,"*Current Breast Cancer Reports*, vol. 2, no.3, 2010, pp.146-151.

[21] D. Di Paolo, et al., "Drug delivery systems: application of liposomal anti-tumor agents to neuroectodermal cancer treatment," *Tumori*, no. 94, no. 2, 2008, pp. 246.

[22] Q Hu, P. S. Kattic and Z. Gu, "Enzyme-responsive nanomaterials for controlled drug delivery," *Nanoscale*, Iss. 21, 2014, pp. 12273-12286.

[23] G. Helmlinger, F. Yuan, M. Dellian and R. K. Jain, "Interstitial pH and pO2 gradients in solid tumors in vivo: high-resolution measurements reveal a lack of correlation," *Nat. Med*., vol. 3, 1997, pp. 177-182.

[24] A. Elegbede, et al., "Mechanistic studies of the triggered release of liposomal contents by matrix metalloproteinase-9," *Journal of the American Chemical Society*, vol. 130, no. 32, 2008, pp. 10633-10642.

[25] R. Cheng, et al., "Dual and multi-stimuli responsive polymeric nanoparticles for programmed site-specific drug delivery," *Biomaterials* vol. 34, no. 14, 2013, pp. 3647-3657.

[26] A. Mitra, C. H. Lee, and K. Cheng, *Advanced Drug Delivery*, y New Jersey: John Wiley & Sons, 2014.

[27] T. M. Allen, and P. R. Cullis, "Liposomal drug delivery systems: from concept to clinical applications," *Advanced drug delivery reviews*, vol. 65, no. 1, 2013, pp: 36-48.

[28] P. P. Deshpande, S. Biswas, and V. P. Torchilin, "Current trends in the use of liposomes for tumor targeting," *Nanomedicine*, vol. 8, no. 9, 2013, pp: 1509-1528.

[29] J. E. Macor, "*Annual reports in medicinal chemistry, Volume 47*, MA, USA: Academic Press, 2012.

[30] J. Jäälinojä, R. Herva, M. Korpela, M. Höyhtyä, and T. Turpeenniemi-Hujanen, "Matrix metalloproteinase 2 (MMP-2) immunoreactive protein is associated with poor grade and survival in brain neoplasms," *Journal of neuro-oncology*, vol. 46, no. 1, 2000, pp. 81-90.

[31] S. M. Janib, A. S. Moses, and J. A. MacKay, "Imaging and drug delivery using theranostic nanoparticles," *Advanced drug delivery reviews*, vol. 62, no. 11, 2010, pp: 1052-1063.

[32] L. Shargel, S. Wu-Pong, and A. B. Yu, *Applied biopharmaceutics & pharmacokinetics*, McGraw-Hill, 2007.

[33] T. Nakano, M. Moore, F. Wei, A.V. Vasilakos, and J. Shuai, "Molecular Communication and Networking: Opportunities and Challenges," *IEEE Transactions on Nanobioscience*, vol 11, no 2, 2012, pp 135-148.

[34] V. Loscrí, C. Marchal, N. Mitton, G. Fortino, and A. V. Vasilakos, "Security and Privacy in Molecular Communication and Networking: Opportunities and Challenges," *IEEE Transactions on NanoBioscience*, vol. 13, no. 3, 2014, pp. 198-207.

[35] T. Nakano, T. Suda, Y. Okaie, M. Moore, and A. Vasilakos, "Molecular communication among biological nanomachines: A layered architecture

and research issues," *IEEE Trans. NanoBiosceience.*, vol. 13, no. 3, 2014, pp. 169-197.

[36] L. Felicetti, M. Femminella, G. Reali, and P. Liò, "Applications of molecular communications to medicine: A survey," *Nano Communication Networks*, doi: 10.1016/j.nancom.2015.08.004.

[37] U.A.K. Chude-Okonkwo, R. Malekian, and B.T. Maharaj, "Diffusion-controlled interface kinetics-inclusive system-theoretic propagation models for molecular communication systems," *EURASIP J. Advances in Signal Processing*, vol. 2015, no. 89, 2015, pp. 1-23.

[38] Y. Chahibi, I. F. Akyildiz, and S. O. Song, "Antibody-based molecular communication for targeted drug delivery systems," In *36th Annual International Conference of the IEEE Engineering in Medicine and Biology Society (EMBC)*,2014 , pp. 5707-5710.

[39] Y. Chahibi, I. F. Akyildiz, S. Balasubramaniam, and Y. Koucheryavy, "Molecular Communication Modeling of Antibody-Mediated Drug Delivery Systems," *IEEE Transactions on Biomedical Engineering*, vol. 62, no.7, 2015, pp.1683-1695.

[40] Y. Chahibi, M. Pierobon, and I. F. Akyildiz, "Pharmacokinetic Modeling and Biodistribution Estimation through the Molecular Communication Paradigm," *IEEE Transactions on Biomedical Engineering*, vol. pp, no.99, pp.1-11.

[41] P. Vanassche, G. Gielen, and W. Sansen, "Symbolic modeling of periodically time-varying systems using harmonic transfer matrices," *IEEE Transactions on Computer-Aided Design of Integrated Circuits and Systems*, vol. 21, no. 9, 2002, p. 1011-1024.

[42] Y. Chahibi, and I. F. Akyildiz, "Molecular communication noise and capacity analysis for particulate drug delivery systems," *IEEE Transactions on Communications*, vol. 62, no. 11, 2014, p. 3891-3903.

[43] A. M. Scott, J. D. Wolchok, and L. J. Old, "Antibody therapy of cancer," *Nature Reviews Cancer*, vol. 12, no. 4, 2012, p. 278-287.

[44] T. Nakano, Y. Okaie, and A. V. Vasilakos, "Transmission rate control for molecular communication among biological nanomachines," *IEEE Journal of Selected Areas in Communication*, vol. 31, no. 12, 2013, pp. 835–846.

[45] L. Felicetti, M. Femminella, G. Reali, T. Nakano, and A. V. Vasilakos, "TCP-like molecular communications," *IEEE Journal of Selected Areas in Communication*, vol.32, no. 12, 2013, pp.2354-2367.

[46] M. Femminella, G. Reali, and A.V. Vasilakos, "A Molecular Communications Model for Drug Delivery," *IEEE Transactions on NanoBioscience*, doi: 10.1109/TNB.2015.2489565.

[47] T. Ruysschaert, M. Germain, J. F.P. Da Silva Gomes, D. Fournier, G. B. Sukhorukov, W. Meier, and M. Winterhalter, "Liposome-based nanocapsules," *IEEE Trans. Nanobioscience*, vol. 3, no. 1, 2004, pp. 49-55.

[48] S. Mura, J. Nicolas, and P. Couvreur, "Stimuli-responsive nanocarriers for drug delivery," *Nature materials*, vol.12, no. 11, 2013, p. 991-1003.

[49] T. L. Andresen, D. H. Thompson, and T. Kaasgaard, "Enzyme-triggered nanomedicine: Drug release strategies in cancer therapy (Invited Review)," *Molecular membrane biology*, vo. 27, no. 7, 2010, p. 353-363.

[50] J. O. You, D. Almeda, J. C. George, and D. T. Auguste, "Bioresponsive matrices in drug delivery," *Journal of biological engineering*, vol. 4, no. 1, 2010, p. 1-12.

[51] D. G. Vartak, and R. A. Gemeinhart, "Matrix metalloproteases: underutilized targets for drug delivery," *Journal of drug targeting*, vol. 15, no. 1, 2007, p. 1-20.

[52] T. Kaasgaard, and T. L. Andresen, "Liposomal cancer therapy: exploiting tumor characteristics," *Expert opinion on drug delivery*, vol. 7, no. 2, 2010, p. 225-243.

[53] J. Banerjee, et al., "Release of liposomal contents by cell-secreted matrix metalloproteinase-9," *Bioconjugate chemistry*, vol. 20, no. 7, 2009, p. 1332-1339.

[54] H. Ishida, et al., "Determining the levels of matrix metalloproteinase-9 in portal and peripheral blood is useful for predicting liver metastasis of colorectal cancer," *Japanese journal of clinical oncology*, vol. 33, no. 4, 2003, p. 186-191.

[55] K. M. Fong, Y. Kida, P. V. Zimmerman, and P. J. Smith, "TIMP-1 an adverse prognosis in non-small cell cancer," *Clin Cancer Res*, vol. 2, 1996, pp. 1369–1372.

[56] G. I. Murray, M. E. Duncan, P. O'Neil, W. T. Melvin, and J. E Fothergill, "Matrix metalloproteinase-1 is associated with poor prognosis in colorectal cancer," *Nat Med*, vol. 2, 1996, pp. 461–462.

[57] B. L. Lokeshwar, "MMP inhibition in prostate cancer," *Ann N Y Acad Sci.*, vol. 878, 1999, pp. 271–289.

[58] A. J. Milici, N. Lhernault, and G. E. Palade, "Surface Densities of Diaphragmed Fenestrae and Transendothelial Channels in Different Murine Capillary Beds," *Circ. Res.*, vol. 56, 1985, pp. 709–717.

[59] F. Alexis, E. Pridgen, L. K. Molnar, and O. C. Farokhzad, "Factors affecting the clearance and biodistribution of polymeric nanoparticles," *Molecular pharmaceutics*, vol. 5, no. 4, 2008, pp. 505-515.

[60] S. Kowalczyk, W., Timothy, R. Blosser and C. Dekker. "Biomimetic nanopores: learning from and about nature," *Trends in biotechnology*, vol. 29, no. 12, 2011, pp. 607-614.

[61] S. P. Adiga, C. Jin, L. A. Curtiss and N, A. Monteiro-Riviere and R. J. Narayan, "Nanoporous membranes for medical and biological applications," *Wiley Interdisciplinary Reviews: Nanomedicine and Nanobiotechnology*, vol. 1, no. 5, 2009, pp.568-581.

[62] Y. W. Yang, "Towards biocompatible nanovalves based on mesoporous silica nanoparticles," *MedChemComm.*, vol. 2, no. 11, 2011, pp. 1033-1049.

[63] V. K. Kumar, "Targeted delivery of nanomedicines," *ISRN pharmacology*, vol. 2012, 2012, pp. 1-9.

[64] W. H. Fissell, H. D. Humes, A. J. Fleischman and S. Roy, "Dialysis and nanotechnology: now, 10 years, or never?" *Blood purification*, vol. 25, no. 1, 2006, pp. 12-17.

[65] M. Pierobon, and I. F. Akyildiz, "Diffusion-based noise analysis for molecular communication in nanonetworks," *IEEE Trans. Signal Processing*, vol. 59, no. 6, 2011, pp. 2532-2547.

[66] V. Malinova, M. Nallani, W. P. Meier and E. K. Sinner, "Synthetic biology, inspired by synthetic chemistry," *FEBS letters*, vo. 586, no. 15, 2012, pp. 2146-2156.

[67] P. D. Rakowska et al., "Nanoscale imaging reveals laterally expanding antimicrobial pores in lipid bilayers," *Proceedings of the National Academy of Sciences*, vol. 110, no. 22, 2013, pp. 8918-8923.

[68] K. Kumar et al., "Formation of nanopore-spanning lipid bilayers through liposome fusion," *Langmuir*, vol. 27, no. 17, 2011, pp. 10920-10928.

[69] F. Haque, J. Li, H.C. Wu, X.J Liang and P. Guo. "Solid-state and biological nanopore for real-time sensing of single chemical and sequencing of DNA," *Nano today*, vol. 8, no. 1, 2013, pp. 56-74.

[70] T. A. Desai et al., "Nanoporous Implants for Controlled Drug Delivery," *BioMEMS and Biomedical Nanotechnology*, 2007, pp. 263-286.

[71] K. E. Orosz et al., "Delivery of antiangiogenic and antioxidant drugs of ophthalmic interest through a nanoporous inorganic filter," *Mol Vis*, vol. 10, 2004, pp. 555-565.

[72] Y. Barenholz, and D. D. Lasic, *Handbook of Nonmedical Applications of Liposomes, Volume 3*, New York: CRC Press, 1996.

[73] E. Elizondo et al., "Liposomes and other vesicular systems: structural characteristics, methods of preparation, and use in nanomedicine," *Progress in molecular biology and translational science*, vol. 104, 2010, pp. 1-52.

[74] G. T. Noble et al., "Ligand-targeted liposome design: challenges and fundamental considerations," *Trends in biotechnology*, vol. 32, no. 1, 2004, pp. 32-45.

[75] P. Yingyuad, et al., "Enzyme-triggered PEGylated pDNA-nanoparticles for controlled release of pDNA in tumors." *Bioconjugate chemistry*, vol. 24, no. 3, 2013, pp. 343-362.

[76] B. Romberg, F. M. Flesch, W. E. Hennink and G. Storm, "Enzyme-induced shedding of a poly (amino acid)-coating triggers contents release from dioleoyl phosphatidylethanolamine liposomes," *Intern.J. Pharmaceutics*, vol. 355, no. 1, 2008, pp. 108-113.

[77] P. Yingyuad et al., "Enzyme-Triggered PEGylated pDNA-Nanoparticles for Controlled Release of pDNA in Tumors,"*Bioconjugate chemistry*, vol. 24, no. 3, 2013, pp. 343-362.

[78] H. ShahMohammadian, G. G. Messier, and S. Magierowski. "Optimum receiver for molecule shift keying modulation in diffusion-based molecular communication channels," *Nano Communication Networks*, vol. 3, no. 3, 2012, pp. 183-195.

[79] B. G. Klein, *Cunnigham's Textbook of Veterinary Physiology*, Missouri, USA: Elsevier Saunders, 2013, pp. 226.

[80] M. Wu, J. Fan, W. Gunning, and M. Ratnam, "Clustering of GPI-anchored folate receptor independent of both-cross-linking and association with caveolin," *The Journal of membrane biology*, vol. 159, no. 2, 1997, pp. 137-147.

[81] K. B. Ghaghada, J. Saul, J. V. Natarajan, R. V. Bellamkonda, and A. V. Annapragada, "Folate targeting of drug carriers: A mathematical model," *Journal of controlled release*, vol. 104, 2005, pp. 113-128.
[82] C. Jeppesen, J.Y. Wong, T.L. Kuhl, J.N. Israelachvili, N. Mullah, S. Zalipsky, and C. M. Marques, "Impact of polymer tether length on multiple ligand-receptor bond formation," *Science*, vol. 293, 2001, pp. 465-468.
[83] W. Ong et al., "Redox-triggered contents release from liposomes." *J. American Chemical Society*, vol. 130, no. 44, 2008, pp. 14739-14744.
[84] M. Afadzi, C. Davies and Y. H. Hansen, "Ultrasound stimulated release of liposomal calcein," in *IEEE Conference on Ultrasonics Symposium (IUS)*, October 2010, pp. 11–14.
[85] B. M. Uzelac, and E. L. Cussler, "Diffusion of small particles through pores of similar diameter," *J. Colloid and Interface Science*, vol. 32, no. 3, 1970, pp. 487-491.
[86] P. Nelson, *Biological physics: energy, information, life*, 1st ed. San Francisco, CA: Freeman, 2008.
[87] D.A. Lauffenburger, and J. Linderman, *Receptors: models for binding, trafficking, and signaling*, Oxford University Press, 1993.
[88] S. Zschiegner, S. Russ, A. Bunde, and J. Kärger, "Pore opening effects and transport diffusion in the Knudsen regime in comparison to self-(or tracer-) diffusion," *Europhysics Letters*, vol. 78, no. 2, 2007, pp. 20001p1-p5.
[89] K. J. Schulten, and I. Kosztin. "Lectures in theoretical biophysics." *University of Illinois* 117, 2000.
[90] P. Bongrand, "Ligand-receptor interactions," *Reports on Progress in Physics*, vol 62, no. 6, 199, pp. 921-968.
[91] S. Shann, et al., "Size-and charge-dependent non-specific uptake of PEGylated nanoparticles by macrophages," *International journal of nanomedicine*, vol. 7, 2012, pp. 799.
[92] M. Longmire, P.L. Choyke, and H. Kobayashi, "Clearance properties of nano-sized particles and molecules as imaging agents: considerations and caveats," *Nanomedicine*, vol. 3, no. 5, 2008, pp. 703–717.
[93] K. Rogers, *The kidneys and the renal system*, NY: Britannica Educational Publishing, 2012.
[94] A. J. Milici, N. Lhernault, and G.E. Palade, "Surface densities of diaphragmed fenestrae and transendothelial channels in different murine capillary beds," *Circ. Res.*, vol. 56, 1985, pp. 709–717.
[95] F. Alexis, E. Pridgen, L.K. Molnar, and O.C. Farokhzad, "Factors affecting the clearance and biodistribution of polymeric nanoparticles," *Molecular pharmaceutics*, vol. 5, no. 4, 2008, pp. 505-515.
[96] S. Ait-Oudhia, D.E. Mager, and R.M. Straubinger, "Application of pharmacokinetic and pharmacodynamic analysis to the development of liposomal formulations for oncology," *Pharmaceutics*, vol. 6, no. 1, 2014, pp. 137-174.
[97] S. Cascone, G. Lamberti, G. Titomanlio, and O. Piazza, "Pharmacokinetics of Remifentanil: a three-compartmental modeling approach," *Translational medicine@ UniSa*, vol. 7, no. 4, 2013, pp. 18-22.